Kinetics of the dehydrogenation of ethylbenzene over uranium oxide containing catalysts

KINETICS OF THE DEHYDROGENATION OF ETHYLBENZENE OVER URANIUM OXIDE CONTAINING CATALYSTS

H.W.G. HEYNEN

KINETICS OF THE DEHYDROGENATION OF ETHYLBENZENE OVER URANIUM OXIDE CONTAINING CATALYSTS

PROEFSCHRIFT

TER VERKRIJGING VAN DE GRAAD VAN DOCTOR IN DE TECHNISCHE WETENSCHAPPEN AAN DE TECHNISCHE HOGESCHOOL EINDHOVEN, OP GEZAG VAN DE RECTOR MAGNIFICUS, PROF.DR.IR. G. VOSSERS, VOOR EEN COMMISSIE AANGEWEZEN DOOR HET COLLEGE VAN DEKANEN IN HET OPENBAAR TE VERDEDIGEN OP DINSDAG 24 SEPTEMBER 1974 TE 16.00 UUR

door

Hubert Wilhelm Gangolf Heynen

geboren te Heinsberg (Dld)

DRUK VAM VOORSCHOTEN

KINETICS OF THE DEHYDROGENATION OF ETHYLBENZENE OVER URANIUM OXIDE CONTAINING CATALYSTS

DIT PROEFSCHRIFT IS GOEDGEKEURD DOOR DE PROMOTOREN:

Prof.Drs.H.S. van der Baan

Prof.Dr.G.C.A. Schuit

aan mijn ouders
aan Yvonne

CONTENTS

CHAPTER 1

INTRODUCTION

1.1. STYRENE MANUFACTURE

Styrene (vinylbenzene, $C_6H_5CH=CH_2$) is one of the oldest and most important basic compounds for the preparation of plastics, such as polystyrene, acrylonitrile-butadiene-styrene terpolymer (ABS), styrene-acrylonitrile copolymer (SAN) and for the production of styrene-butadiene synthetic rubber.

In 1839, Simon (1) described the distillation of a natural balsamic material - storax - whereby the distillate separated into water and an "essential oil", for which he proposed the name "Styrol". In 1867, Berthelot made styrene, among other products, by passing benzene and ethylene through a red hot tube (2,3) and thus showed the way to the industrial process used today.

Although styrene was known to polymerize, no commercial applications were attempted for many years because the polymers were brittle and cracked easily. But about 1925, when the I.G. Farbenindustrie discovered the useful properties of butadiene-styrene copolymer, the development of a styrene process became attractive. A process for the manufacture of styrene by the dehydrogenation of ethylbenzene was developed simultaneously by the Dow Chemical Company and the Badische Anilin- und Soda Fabrik A.G. and in 1937 both companies were manufacturing a high purity monomer. The demand for synthetic rubber during the Second World War stimulated styrene production enormously. Especially during the last twenty years the styrene production has expanded rapidly; in the U.S. only the production reached 5900 million pounds in 1972. Surveys of the

development of the styrene manufacture have been given by Ohlinger (4) and by Miller (5).

The most important commercial process at present is the direct dehydrogenation of ethylbenzene. A survey of the literature of dehydrogenation catalysts up till 1955 has been given by Kearby (6). At present, catalysts on iron-chromium oxide basis, like for instance the Shell 105 catalyst, containing 93% Fe_2O_3, 5% Cr_2O_3 and 2% KOH, are believed to be in general use.

The catalytic dehydrogenation of ethylbenzene

$$C_6H_5C_2H_5 \rightleftharpoons C_6H_5CH{=}CH_2 + H_2 \qquad \Delta H^{\circ}_{900} = 29.8 \text{ kcal mol}^{-1}$$

is carried out at 600-650°C using large amounts of steam as diluent. Another important role of the steam is keeping the catalyst active because deposited coke is removed by the water gas reaction:

$$C + 2H_2O \rightarrow CO_2 + 2H_2 \qquad \Delta H^{\circ}_{900} = 23.8 \text{ kcal mol}^{-1}$$

For the commercial process ethylbenzene conversions higher than 40% are not allowed, since the selectivity for styrene, usually about 92%, decreases rapidly with increasing conversions. The following side reactions take place:

$$C_6H_5C_2H_5 \rightarrow C_6H_6 + C_2H_4 \qquad \Delta H^{\circ}_{900} = 24.3 \text{ kcal mol}^{-1}$$

$$C_6H_5C_2H_5 + H_2 \rightarrow C_6H_5CH_3 + CH_4 \qquad \Delta H^{\circ}_{900} = -15.4 \text{ kcal mol}^{-1}$$

$$C_6H_5C_2H_5 + H_2 \rightarrow C_6H_6 + C_2H_6 \qquad \Delta H^{\circ}_{900} = -10.0 \text{ kcal mol}^{-1}$$

In addition to benzene and toluene, very small amounts of cumene and α-methylstyrene are found in the product mixture.

Recently a few remarkable oxidative dehydrogenation processes have been described. For instance, the Halcon International Company has started a process (7) in which ethylbenzene is oxidized to ethylbenzene hydroperoxide:

$$C_6H_5C_2H_5 + O_2 \rightarrow C_6H_5CH(OOH)CH_3$$

This product reacts with propylene to give propylene oxide and 1-phenylethanol, after which the alcohol is dehydrated to styrene. Adams (8) describes a process in which ethylbenzene is oxidatively dehydrogenated on phosphate catalysts with sulfurdioxide at 450-600°C. Conversions of approximately 80-90% are reached with selectivities of the same order of magnitude, but at present there are no commercial styrene plants utilizing this process.

1.2. URANIUM OXIDE AS DEHYDROGENATION CATALYST

In 1972 Steenhof de Jong (9) described a reaction to produce benzene by passing toluene over bismuth uranate, Bi_2UO_6, at 400-500°C. Bismuth uranate acts as an oxidant in this reaction and the toluene conversion stops when the uranate is reduced. Attempts to dealkylate ethylbenzene with this compound as well were successful under similar reaction conditions, but the selectivity for benzene was less than 50%; other reaction products were CO_2, H_2O, H_2, styrene and toluene. It turned out, however, that in this case the reaction does not stop when bismuth uranate is completely reduced to metallic bismuth and UO_2, but considerable amounts of styrene and hydrogen were formed with high selectivity (10).

Further investigations showed that pure uraniumdioxide is an at least as active and more stable dehydrogenation catalyst. Only in the older literature is uraniumtrioxide

mentioned as component of ethylbenzene dehydrogenation catalysts (11) or as a promotor for these catalysts (12). The activity and the mechanical strength of the catalyst is highly increased when uranium oxide is brought on alumina. This catalyst gave conversions of 80% with styrene selectivities of over 95% at reaction temperatures of about 500°C. Because of these remarkable results we decided to study the dehydrogenation of ethylbenzene over the uranium oxide catalysts in the absence of steam.

1.3. DEHYDROGENATION KINETICS

In spite of the importance of the ethylbenzene dehydrogenation process and the considerable number of publications on the technical performance and on the dehydrogenation catalysts, very little kinetic data have been published so far.

Wenner (1948,13) described the results of industrial catalytic dehydrogenation experiments with the simple equation for equilibrium reactions:

$$r = k(c_{EB} - c_{St}c_H/k_{eq}) \qquad (1.1)$$

Balandin (1958,14) gave the rate equations for a number of dehydrogenation reactions.
The ethylbenzene dehydrogenation rate was found to be:

$$r = k\frac{c_{EB}}{\sum_i K_i c_i} \qquad (1.2)$$

The denominator of equation 1.2 corresponds to Langmuir's adsorption isotherm for mixtures; K_i represent the relative adsorption coefficients.

Finally, Carrà (1965, 15) used for his experiments with the Shell 105 catalyst an equation combining the features of 1.1 and 1.2:

$$r = \frac{k(c_{EB} - c_{St}\, c_H / k_{eq})}{1 + KE\, c_{EB} + KS\, c_{St}} \qquad (1.3)$$

No hydrogen adsorption term is present in the denominator because at the reaction temperatures (about 600°C) hydrogen adsorption is thought to be negligible. With this equation Carrà was able to describe the experimental data satisfactorily, except at temperatures above 630°C, where by-product formation becomes important.

LITERATURE CHAPTER 1

1. Simon, E., Justus Liebigs Ann. Chem. 31, 265 (1839).
2. Berthelot, M., Justus Liebigs Ann. Chem. 142, 257 (1867).
3. Berthelot, M., Bull. Soc. Chim. Fr. 10, 341 (1868).
4. Ohlinger, H., and Stadelmann, S., Chem.-Ing.-Tech. 37, 361 (1965).
5. Miller, S.A., and Donaldson, J.W., Chem. Process Eng. 48(Dec), 37 (1967).
6. Kearby, K.K., "Catalysis" Vol. III, Reinhold Publishing Corp., New York (1955).
7. Halcon International, Netherlands Pat. 6,500,118 and 6,515,037 (1966).
8. Adams, C.R., and Jennings, T.J., J. Catal. 17, 157 (1970).
9. Steenhof de Jong, J.G., Guffens, C.H.E., and van der Baan, H.S., J. Catal. 26, 40 (1972).

10. Heynen, H.W.G., and van der Baan, H.S., J. Catal. in press.
11. Steiner, H., and Whincup, S., British Pat. 576,416 (1946).
12. Graves, G.D., U.S. Pat. 2,036,410 (1936).
13. Wenner, R.R., and Dybdal, E.C., Chem. Eng. Progr. 44, 275 (1948).
14. Balandin, A.A., Advan. Catal. 10, 96 (1958).
15. Carrà, S., and Forni, L., Ind. Eng. Chem., Process Des. Develop. 4, 281 (1965).

CHAPTER 2

APPARATUS AND ANALYSIS

2.1. INTRODUCTION

The study of the ethylbenzene dehydrogenation over uranium oxide was started in a fixed bed tubular reactor. In this reactor catalyst reduction, catalyst lifetime and the influence of reaction conditions on conversion and selectivity were investigated. Tests for diffusion limitation and differential measurements were also carried out.

Experiments with a plug flow reactor, however, may be less accurate, because mass and heat transport effects may go unnoticed. High feed flow rates will alleviate these problems, but the resulting low conversion will introduce inaccuracies in the analysis. We therefore decided to build a continuous stirred gas solid reactor (CSGSR), where high internal flow rates can be combined with high conversion of the outside feed. A survey of the different types of stirred gas solid reactors developed has been given by Choudhary (1). Instead of a spinning basket we decided to apply in our CSGSR forced circulation of the gas phase through a stationary bed, because this allows of easy measurement of the bed temperature and of the pressure drop over the bed. Especially the latter information is important as this allows calculation of the flow rate through the bed.

We were confident that the combined information from plug flow reactor and CSGSR, as advocated by Kiperman (2), would allow us to determine the dehydrogenation kinetics more accurately. Experiments with our first CSGSR, reactor A, showed that there were discrepancies between the performance of this reactor and that of the tubular reactor

which could not be explained on theoretical grounds. These differences have been ascribed, at least for a major part, to the fact that the catalyst in both reactors had a different history. To ascertain that the conditions in the tubular reactor and the CSGSR were fully comparable, we finally developed a new reactor, reactor B, in which reactions under both plug flow and CSGSR conditions could be carried out on the same quantity of catalyst and which could be switched over easily from the one mode of operation to the other. The final kinetic experiments were carried out in this reactor.

All experiments were performed under continuous flow conditions. The products were analyzed by an on-line gas-chromatographic system. With this system all components of the product gas were determined, except water which is formed during the reduction of the catalyst and small amounts of light hydrocarbons, formed together with the by-products benzene and toluene.

The reduction behaviour of the catalyst was determined in a thermobalance. The degree of reduction was also calculated from the quantities of the oxygen containing products formed during the reduction.

2.2 THE REACTION SYSTEM

In figure 2.1 a diagram of the apparatus is given.A constant flow of carrier gas (nitrogen or carbondioxide), carefully freed from oxygen by reduced BASF R3-11 catalyst, passes through one of the vaporizers (V_1 and V_2), filled with ethylbenzene or a mixture of ethylbenzene and styrene respectively.

The desired ethylbenzene concentration in the feed gas is established by adjusting the temperature of vaporizer V_1, which is controlled within $0.2^{o}C$. The gas leaving the

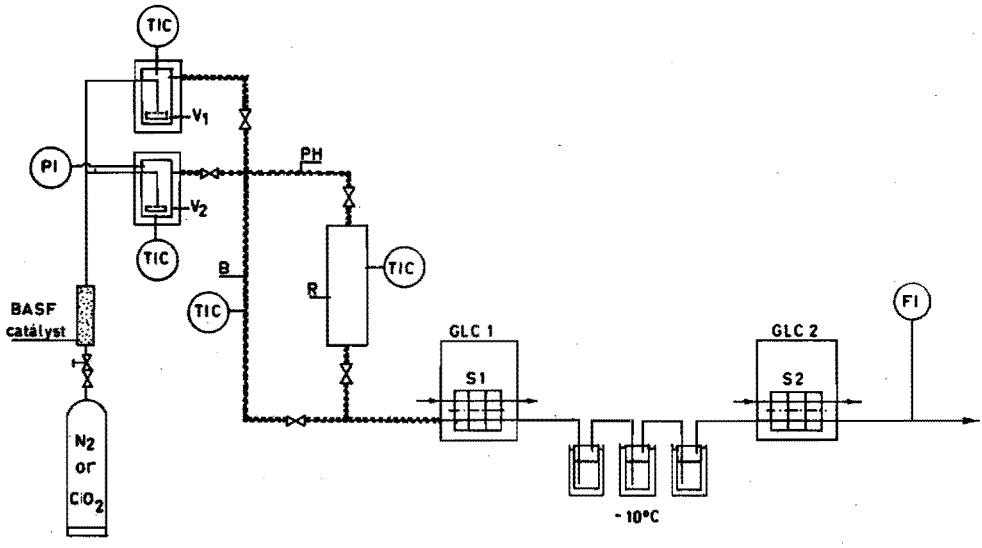

Fig. 2.1 Apparatus.

vaporizer is completely saturated as was confirmed by condensing the ethylbenzene at -80°C. The amounts of styrene and ethylbenzene in the feed, when the carrier gas is led through V_2, were determined by comparing peak areas with those obtained from known concentrations of ethylbenzene.

The mixture of carrier gas and hydrocarbon passes either via preheater PH through reactor R to sample valve S_1 (3) or directly via bypass B to that valve. The connecting tubes between the vaporizer and S_1 are heated to prevent condensation of hydrocarbons. Feed or products are introduced by means of the valves S_1 and S_2 in an analysis system, consisting of two gaschromatographs, GLC_1 and GLC_2, separated by cold traps to condense the hydrocarbons analyzed on GLC_1.

Two identical systems, one with the tubular reactor and the other with the CSGSR, were in operation.

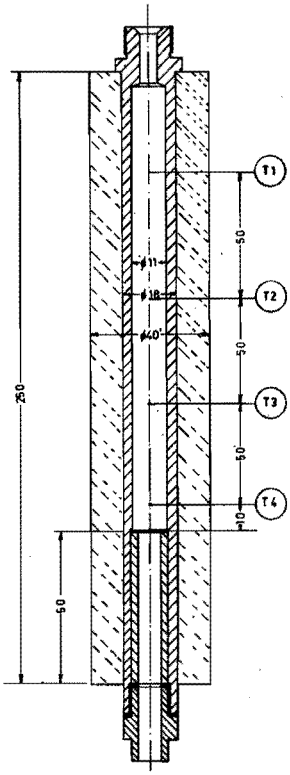

Fig. 2.2 Tubular fixed bed reactor.

The tubular reactor is shown in figure 2.2. Round the stainless steel reactor tube an aluminium jacket has been cast to improve the temperature profile in the reactor. The reactor is heated electrically; the temperature is measured and controlled within 1°C by a Eurotherm PID controller. Under the reaction conditions the maximum temperature difference between the four chromel-alumel thermocouples was never more than 2°C. The catalyst is supported by a fine-meshed wire screen.

Figure 2.3 shows the stainless steel CSGSR, reactor A, including the stirrer drive unit, which has been constructed similarly to the unit described by Brisk (4). The completely sealed, magnetically coupled drive was capable of rotating at speeds up to 10,000 rpm.

This necessitated dynamical balancing of the fan and the driving shaft. In reactor A the annular catalyst holder A was used. Reactor B and catalyst holder B are shown in figure 2.4. When the plug is in its lower position the gas circulates through the reactor in the same way as in reactor A. By turning the spindle the plug closes the central hole of the catalyst holder and then no internal recirculation is possible anymore . The gas feed passes once through the catalyst bed in plug flow fashion. The bellows serve as a flexible sealing. The reactor proper is placed in an oven, kept at about 20°C below the desired reaction temperature. This temperature is measured and controlled by a Eurotherm

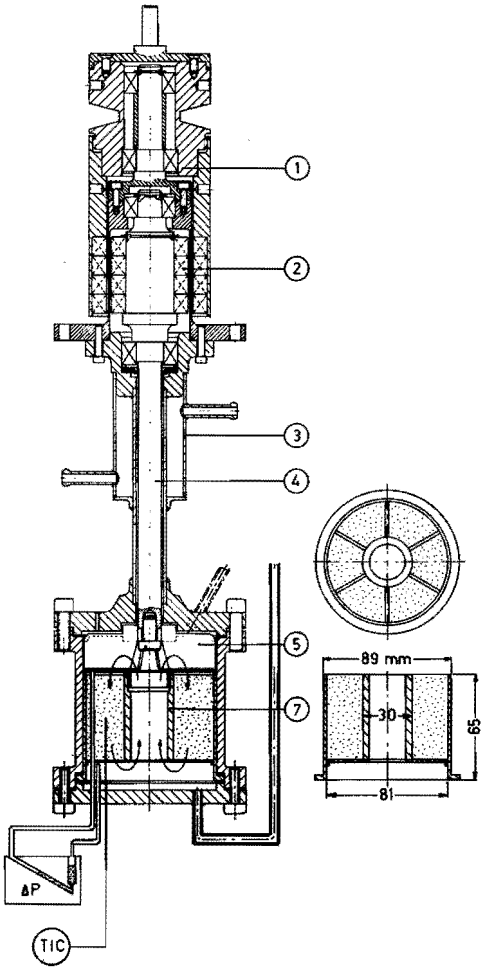

Fig. 2.3 Continuous stirred gas solid reactor (A) and catalyst holder A

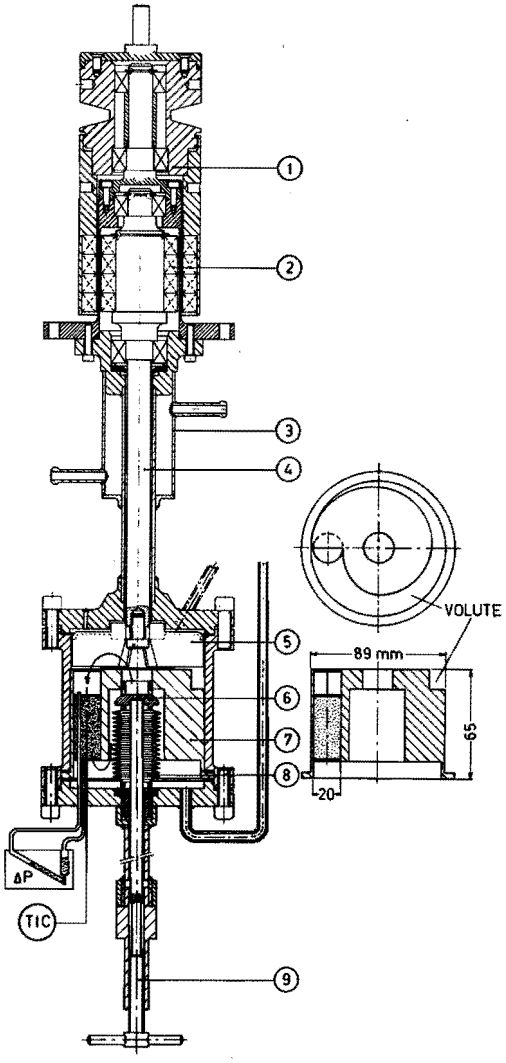

Fig. 2.4 Continuous stirred gas solid reactor (B) and catalyst holder B

1 pulley; 2 magnet; 3 air cooler; 4 drive shaft; 5 fan; 6 plug; 7 catalyst holder; 8 bellows; 9 spindle.

PID controller which governs the amperage of the auxiliary heating coil round the reactor.

2.3 ANALYSIS

The hydrocarbons, benzene, toluene, ethylbenzene and styrene in the reaction product were analyzed on GLC_1, a Pye series 104 gaschromatograph with flame ionization detector. The separation column, 2 m long, internal diameter 2 mm, was filled with 20 wt% polyethylene glycol adipate on Gaschrom Q and kept at 120 °C. A chromatogram of a typical sample is shown in figure 2.5. The analysis time is 3 minutes.

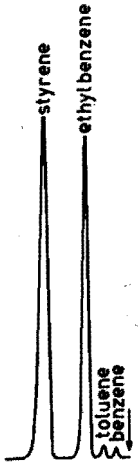

Fig. 2.5 Chromatogram of ethylbenzene dehydrogenation product mixture.

By injecting benzene, toluene, ethylbenzene and styrene mixtures of known composition, it was found that the detector sensitivities (signal per unit weight of hydrocarbon) were equal. The following relation can be derived for the quantitative determination of the reaction products:

$$x_i = \gamma_i \frac{A_i}{A_{EB_o}} x_{EB_o} \qquad \text{with } \gamma_i = MW_i \,/\, MW_{EB}$$

in which:
- x_i = mole fraction of component i
- MW = molecular weight
- A_i = peak area of component i
- A_{EB_o} = peak area of a sample with only ethylbenzene with mole fraction x_{EB_o}

As the number of moles in the reaction system increases, the mole fractions have to be corrected to the actual conditions in the reactor as is pointed out in Appendix I. Introduction of average values for the increment in the number of moles instead of the actual ones, does not lead to inaccuracies of any importance. For low vapour pressure and low conversions this correction is negligible.

On GLC_2, a Becker gaschromatograph with katharometer detector, hydrogen and carbondioxide (only present during reduction of the catalyst) were determined using a 20 cm active charcoal column, kept at $66^{o}C$. The ethylbenzene carrier gas and the carrier gas for GLC_2 were identical and therefore, after reduction of the catalyst, only a hydrogen peak was recorded.

For the quantitative determination of hydrogen and carbondioxide the relations:

$$x_{H_2} = f_{H_2} A_{H_2} \quad \text{and} \quad x_{CO_2} = f_{CO_2} A_{CO_2} \quad \text{were used.}$$

The response factors f were determined by analyzing gas mixtures of known composition under standard chromatograph conditions. The mixtures of CO_2 and H_2 and nitrogen and of H_2 and carbondioxide were obtained with two Wösthoff plunger pumps.

2.4. THERMOBALANCE

In figure 2.6 the Dupont 900/950 thermobalance that we used is shown. The sample chamber is a 4 cm i.d. quartz glass tube, heated by an electric furnace. The sample chamber is flushed with a hydrogen nitrogen mixture or an ethylbenzene nitrogen mixture prepared as described in § 2.2. The temperature of the chamber is measured with a thermocouple just above the sample holder.

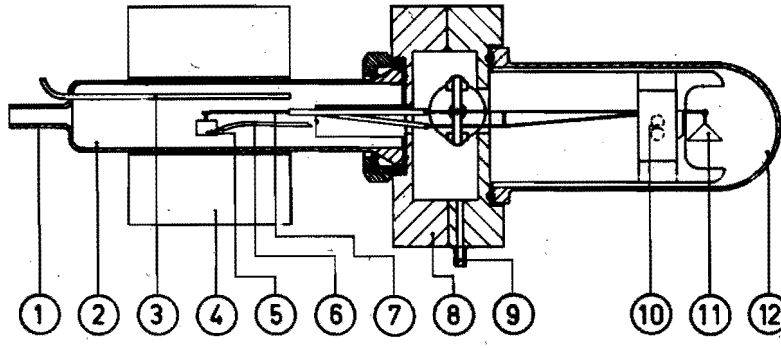

Fig. 2.6 Thermobalance:
1 feed gas inlet; 2 furnace tube; 3 gas outlet;
4 furnace; 5 sample holder; 6 thermocouple;
7 quartz glass tube; 8 balance housing;
9 purge gas inlet; 10 photo-voltaic cells;
11 counter weight pan; 12 pyrex envelope.

The part of the balance where the weight changes are recorded with photocells, is purged with nitrogen to avoid contamination. To prevent back diffusion of air the gas outlet tube ends under water.

The sensitivity of the thermobalance is 0.01 mg. With the usual sample weight of 80 mg this corresponds to an error in the degree of reduction of pure uranium oxide of 0.3% and of uranium oxide on alumina of 1.1%.

LITERATURE CHAPTER 2

1. Choudhary, V.R., and Doraiswamy, L.K., Ind. Eng. Chem., Process Des. Develop. 11, 420 (1972).
2. Kiperman, S.L., Kinet. Katal. 13, 562 (1972).
3. German, A.L., and Heynen, H.W.G., J. Sci. Instrum. 5, 413 (1972).
4. Brisk, M.L., Day, R.L., Jones, M., Warren, J.B., Trans. Inst. Chem. Eng. 46(1), T3 (1968).

CHAPTER 3

PREPARATION AND PROPERTIES OF URANIUM OXIDE CONTAINING CATALYSTS

3.1. INTRODUCTION

The oxides of uranium form a complex system, often showing large deviations from simple stoichiometry. The stoichiometric oxides include UO_2, U_4O_9, U_3O_8 and UO_3. In addition, metastable phases, such as U_3O_7 and U_2O_5 have been reported (1). Uraniumdioxide is of particular interest in nuclear technology, since it is the nuclear fuel most widely used in energy-producing reactors. The investigations published on the uranium-oxygen system until 1969 have been reviewed by Cordfunke (2). Some properties of uranium oxide compounds are given in table 3.1.

Of the oxide UO_3 at least six crystalline polymorphs, and also an amorphous form are known. Upon heating in air, both α-UO_3 and β-UO_3 are converted into γ-UO_3, indicating that under these conditions γ-UO_3 is the stable configuration. γ-UO_3 can be prepared by slowly heating uranylnitrate to 500°C.

The oxide U_3O_8 exists in at least three crystallographic modifications, but α-U_3O_8 is the phase commonly dealt with. It is the form of the oxide most frequently weighed in gravimetric uranium analysis. Its composition remains close to $UO_{2.67}$ below a temperature of 800°C. β-U_3O_8 often occurs as a contamination in α-U_3O_8, while γ-U_3O_8 can only be made at very high oxygen pressures (>16,000 atm) between 200 and 300°C.

UO_2 has a face-centered cubic fluorite-type structure. It is generally made by reduction of UO_3 at 650-800°C. This oxide cannot be further reduced, not even with hydrogen at high pressure and temperature.

Table 3.1 Properties of uranium oxide phases (from(2)).

phase	structure	$-\Delta Hf^{o}_{298}$	S^{o}	colour
		kcal mol^{-1}	cal $(^{o}mol)^{-1}$	
UO_2	cubic a= 5.47 Å	259	18.41	black
α-U_4O_9	cubic a= 21.77 Å	1078	83.53	black
α-U_3O_8	orthorhombic a= 6.72 Å b= 11.96 Å c= 4.15 Å	854	67.5	dark green
γ-UO_3	monoclinic, pseudo-tetragonal a=b=6.89 Å c= 19.94 Å γ= 90.34	293.5	23.6	orange-yellow

If UO_2 takes up oxygen the disordered UO_{2+x} phase changes to a new phase, U_4O_9 if x = 0.25.

3.2. CATALYST PREPARATION

Preparation of pure uranium oxide catalyst (Catalyst A)

Uranylacetate ($(CH_3COO)_2UO_2.2H_2O$ Merck p.a.) is dissolved in hot water. An excess of a concentrated ammonia solution is added and the yellow precipitate $UO_3.xNH_3.yH_2O$ (3) is filtered off and washed with water. The precipitate

is dried at 135°C during 24 h and the product is finally calcined at 600°C for 24 h. The dark green product is broken and sieved.

Preparation of uranium oxide/alumina catalyst (Catalyst B)

The precipitate $UO_3.xNH_3.yH_2O$, starting from 20 g uranylacetate, is prepared as mentioned before. 409 g aluminiumnitrate ($Al(NO_3)_3.9H_2O$ Merck p.a.) is dissolved in water and poured into 300 ml of concentrated ammonia solution. The precipitate is filtered off and washed with water. The two precipitates are transferred to a flask, mixed with 1 l of water, and kept at 95-100°C under vigorous stirring. After 20 h of stirring the solid is filtered off, washed with water and dried for 24 h at 135°C. Finally the product is calcined at 600°C in air for 24 h and the resulting catalyst is broken and sieved.

3.3. PHYSICAL PROPERTIES

Some properties of the catalysts are summarized in table 3.2.

X-ray diffraction diagrams were made with a Philips diffractometer, using iron filtered cobalt radiation. The spectrum of the pure uranium oxide shows γ-U_3O_8 lines and very weak α-UO_3 lines. Catalyst B was amorphous. The colours and the O/U ratios indicate that uranium oxide in the catalysts A and B is mainly present in the U_3O_8 and the UO_3 configuration respectively. The pore size distribution of the alumina supported catalyst was measured according to the Barrett,Joyner and Halenda method using nitrogen as

Table 3.2 Properties of catalyst A and B.

	pure uranium oxide catalyst A	uranium oxide on alumina catalyst B
colour	dark green	orange-yellow
oxygen/uranium ratio of the oxide	2.71	2.87
uranium oxide content (wt%)	100	19.4
specific surface area BET using nitrogen adsorption ($m^2\ g^{-1}$)	6.3	144

adsorbent. From figure 3.1 we can conclude that 90% of the pore volume consists of pores with a radius smaller than 50 Å. From this experiment a surface area of 150 $m^2\ g^{-1}$ was found. This is in good agreement with the value given in table 3.2, which has been determined with an areameter. The average pore radius calculated with the relation:

$$\text{pore radius} = \frac{2 \times \text{pore volume}}{\text{surface area}}$$

was 46 Å.

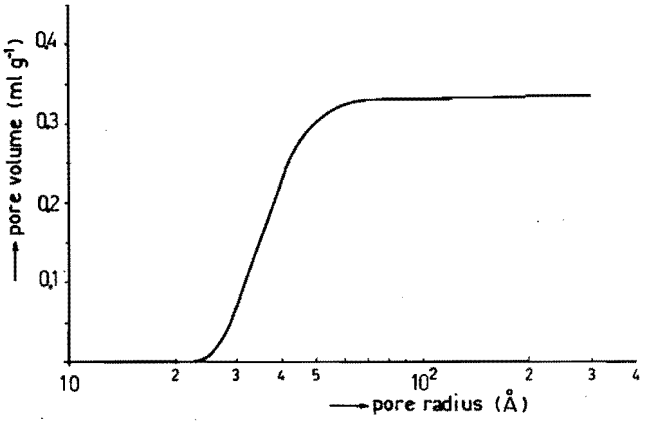

Fig. 3.1 Cumulative volume of pores having a radius smaller than r_p as a function of r_p.

3.4. THE REACTION BETWEEN ETHYLBENZENE AND URANIUM OXIDE

When ethylbenzene in inert gas is led over bismuthuranate (4) at temperatures of about 480°C, reactions similar to those described by Steenhof de Jong (5,6) take place. During this reaction, bismuthuranate is reduced and water, carbondioxide, benzene and styrene are formed. When the uranate is completely reduced, the products are almost exclusively styrene and hydrogen.

During the reduction of pure uranium oxide or uranium oxide on alumina with ethylbenzene, the product composition changes in a similar way as with bismuthuranate, but the reduction proceeds at a higher rate. The change of the product composition in a typical reduction experiment of catalyst A is shown in figure 3.2. The reaction starts with complete combustion of ethylbenzene to CO_2 and water. Very soon the formation of benzene by oxidative dealkylation is observed, while the styrene formation starts somewhat later. Hydrogen, formed together with styrene, is partly oxidized to H_2O initially, but after completion of

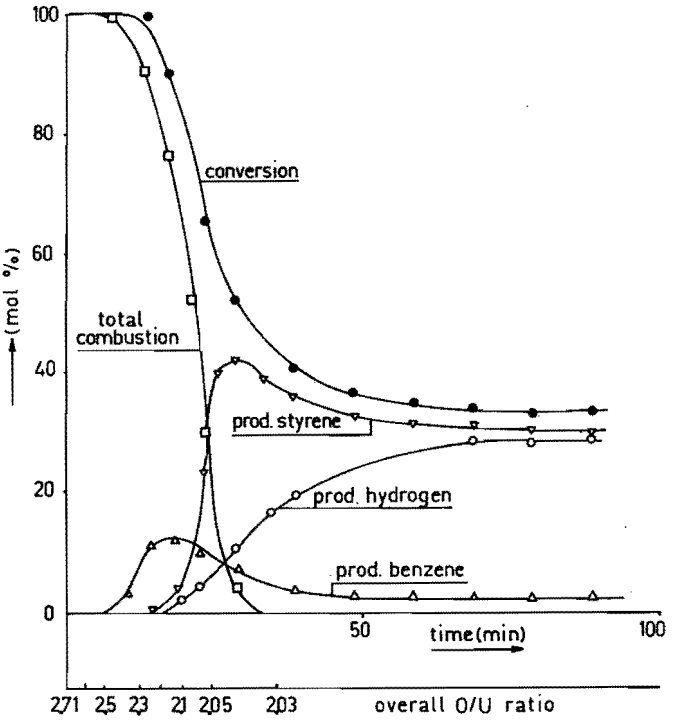

Fig. 3.2 Product composition change during the reduction of catalyst A: reaction temperature 500°C; catalyst weight 1 g; feed 2.5 l h^{-1} N_2 and 0.327 mmol h^{-1} ethylbenzene.

the reduction the amounts of hydrogen and styrene in the product are equal. The partial oxidation of hydrogen causes the maximum in the styrene production, as this oxidation reduces the rate of the hydrogenation reaction. Small amounts of benzene and toluene, formed over completely reduced catalyst, are probably caused by hydrodealkylation and cracking. During reduction, catalyst A turns from green to black and catalyst B, originally orange, first becomes green and finally black. Reduction with hydrogen gives the same colour change. As on reoxidation the original colours return, we conclude that the different colours must be ascribed to different stages of reduction.

The amount of oxygen removed from the catalyst was calculated from the quantities of the various products assuming the following reactions:

$$C_8H_{10} + 21\,[O] \rightarrow 8\,CO_2 + 5\,H_2O$$

$$C_8H_{10} + 6\,[O] \rightarrow C_6H_6 + 2\,CO_2 + 2\,H_2O$$

$$C_8H_{10} + [O] \rightarrow C_8H_8 + H_2O$$

and thus the course of the overall O/U ratio of the catalyst during the reduction, as shown in figure 3.2 was determined.

During reduction of catalyst B the hydrocarbon product composition changes in a way almost identical with that described for catalyst A.

We have not made X-ray diagrams of the solid phases formed during the reduction, because special techniques have to be applied, as rapid reoxidation of the material takes place even at room temperature.

3.5. THE REDUCTION OF PURE U_3O_{8+x} AND URANIUM OXIDE ON ALUMINA IN A THERMOBALANCE

Freshly prepared dehydrogenation catalyst contains U_3O_8, with a small excess of oxygen, which is reduced to UO_2 by ethylbenzene under reaction conditions as stated before. The degree of reduction and the reduction rate of both pure uranium oxide and uranium oxide on alumina can be measured continuously and accurately in a thermobalance. The reaction conditions for experiments with pure oxide are given in table 3.3.

Under these conditions no gas phase diffusion limitation occurs as the reduction rates are not affected by an increased gas flow rate nor by the particle size.

Table 3.3 Thermobalance reaction conditions.

amount of oxide	70-80 mg
particle size	0.15-0.30 mm
mole fraction ethylbenzene	0.26-5.2 mol %
nitrogen flow	13.3 l h^{-1} NTP
reaction temperature	425-530°C
pressure	atmospheric

Neither does hydrocarbon adsorption influence the measurements, since complete reduction with ethylbenzene and with hydrogen give the same weight loss.

From complete reduction experiments a O/U ratio 2.71 was determined for pure uranium oxide, while for uranium oxide in catalyst B a ratio 2.87 was found.

3.5.1. PURE URANIUM OXIDE REDUCTION

The effect of the ethylbenzene concentration on reduction of pure uranium oxide is shown in figure 3.3. In the first region (A) a very high, but rapidly declining, reduction rate occurs. This region ends at a catalyst composition $UO_{2.6}$ (α = 13%). In the next region (B) the reduction rate is constant for all ethylbenzene concentrations. This region ends at catalyst composition $UO_{2.25}$ (α = 67%). Finally the rate decreases again in region C.

In figure 3.4 log(-dO/dt) in region B has been plotted against log x_{EB}. With the relation

$$-dO/dt = k\, x_{EB}^{n} \quad \text{or} \quad \log(-dO/dt) = n \log x_{EB} + C$$

we can read from this figure that n is about 0.2 at x_{EB} = 0.26 mol % and that for x_{EB} > 0.6 mol % n=0.

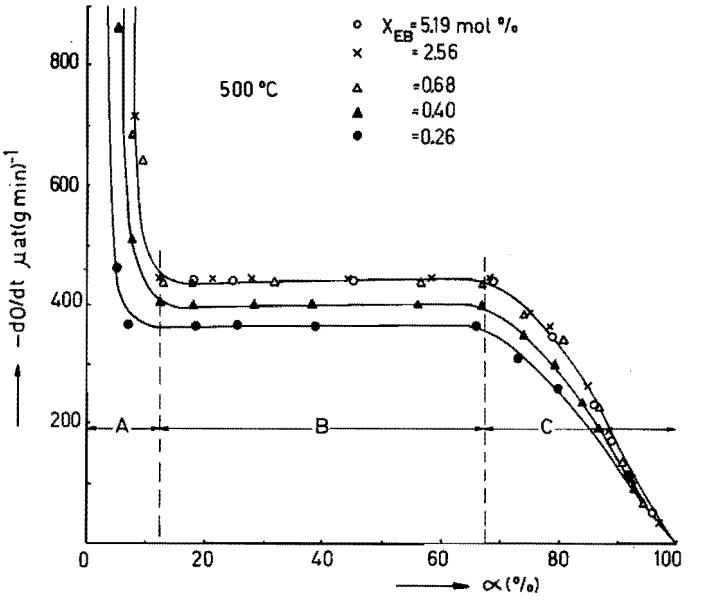

Fig. 3.3 Reduction rate as a function of the degree of reduction α at various ethylbenzene mole fractions.

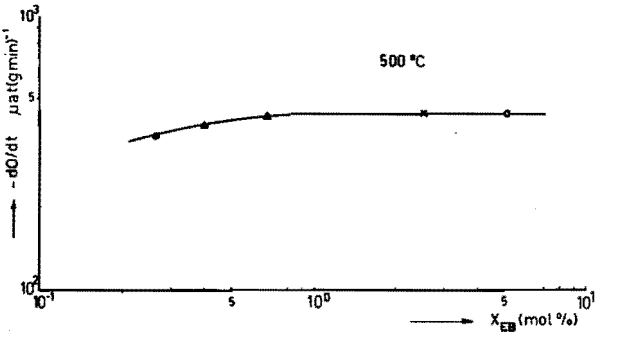

Fig. 3.4 Reduction rate in region B as a function of the ethylbenzene mole fraction.

The effect of the reaction temperature was studied at an ethylbenzene mole fraction of 0.68%. In figure 3.5 the rates of reduction as a function of the degree of reduction at various temperatures are given. Here again the three regions can be clearly distinguished and it is remarkable that the extent of region B (13% < α < 67%) is also

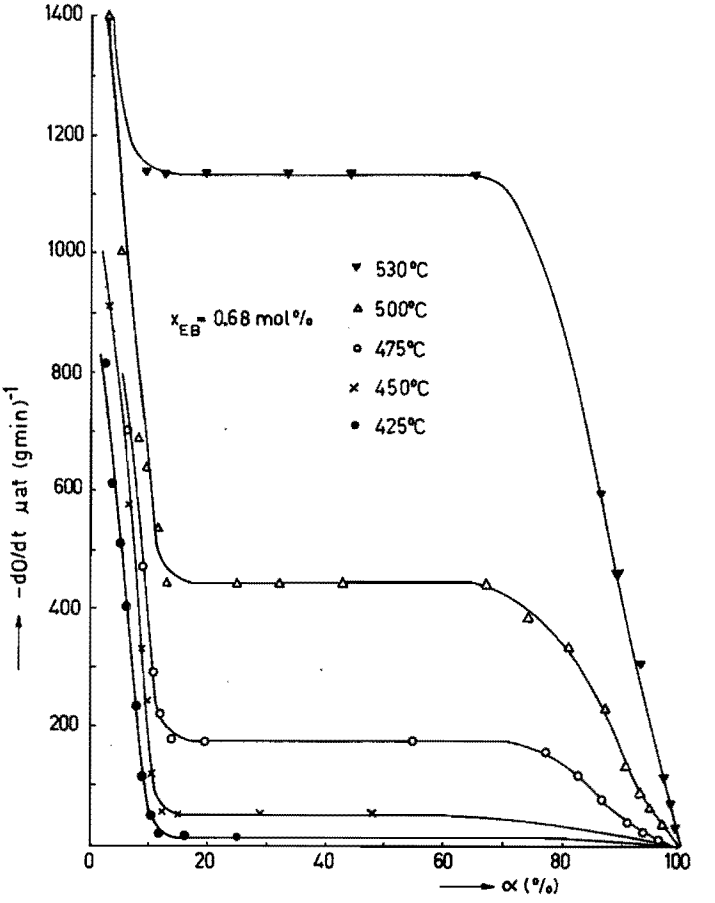

Fig. 3.5 Reduction rate as a function of the degree of reduction α at various temperatures; reduction with ethylbenzene.

independent of the temperature. From the rates in this region an activation energy of 46 kcal mol^{-1} was calculated from figure 3.6.

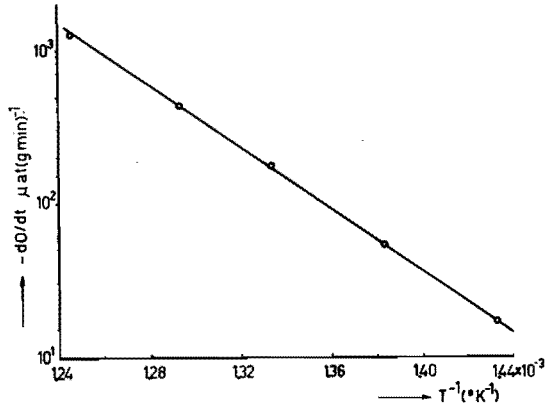

Fig. 3.6 Arrhenius plot for the rate of reduction in region B; reduction with ethylbenzene.

The catalysts were also reduced with a nitrogen hydrogen mixture containing 10 to 60 mol % hydrogen. The other conditions were the same as shown in table 3.3. The results of the reduction of catalyst A with hydrogen (figure 3.7 and 3.8) are similar to those mentioned above. Here again the reduction rate remains constant for $13\% < \alpha < 67\%$, but the reaction order for hydrogen is very close to 1 now, as can be seen from figure 3.9. The energy of activation (figure 3.10) was 29 kcal mol^{-1}.

A reduction behaviour very similar to the above was also noticed by Steenhof de Jong (5, 6) for the reduction of Bi_2UO_6 with toluene. The appearance of different regions during the reduction of uraniumtrioxide is also mentioned by Notz (7) and Vlasov (8, 9). For hydrogen reduction Notz found also three regions with the same properties as we did, although the extent of the regions differs somewhat from ours. He found region A between $UO_{2.7}$ and $UO_{2.6}$, and

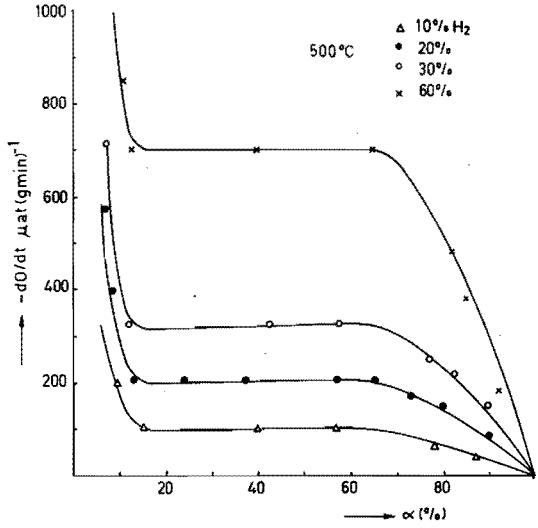

Fig. 3.7 Reduction rate as a function of the degree of reduction α at various hydrogen mole fractions.

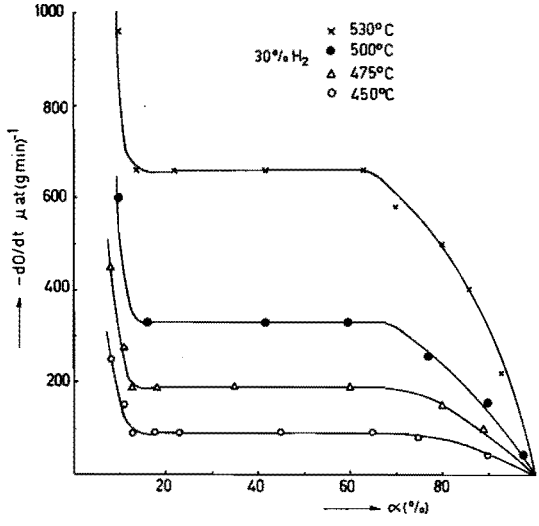

Fig. 3.8 Reduction rate as a function of the degree of reduction α at various temperatures; reduction with hydrogen.

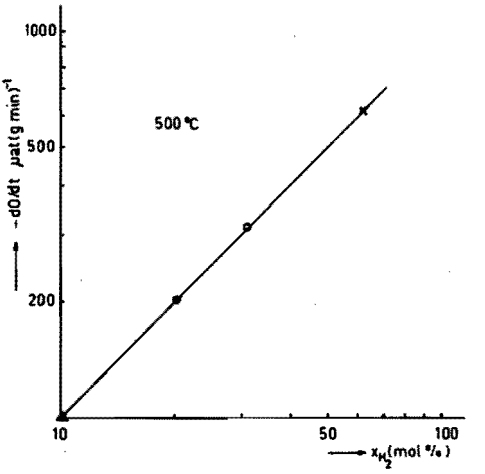

Fig. 3.9 Reduction rate in region B as a function of the hydrogen mole fraction.

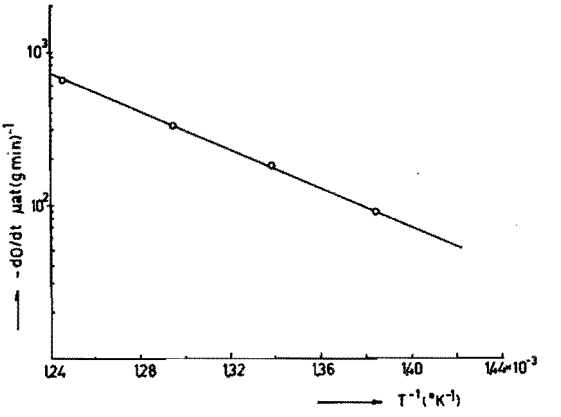

Fig. 3.10 Arrhenius plot for the rate of reduction in region B; reduction with hydrogen.

region B between $UO_{2.6}$ and $UO_{2.2-2.1}$. In region A, a homogeneous transition from the upper to the lower composition limits of the U_3O_8 structure occurs. In region B, U_3O_{8-x} is converted into a cubic structure. The author explains the constant rate by assuming chemisorption of hydrogen as a rate limiting step, while oxygen diffuses through the solid to the surface as fast as it is abstracted. The final decrease in the rate is attributed to non uniform crystallite size or poor gas accessibility to the centers of some large particles. However, we believe that the sharp transition between the three regions A, B and C and the fact that the positions of the transition points are independent of the reaction conditions, indicate that the crystallite size distribution is rather narrow. Another possible explanation of these phenomena is that oxygen diffuses easily from one crystallite to another via planes of contact. This would mean that, as far as oxygen diffusion in the catalyst is concerned, each particle acts as if it consists of only one crystallite, and therefore the crystallite size distribution should not be important in this case. We shall return to this subject in the description of catalyst B reduction. Vlasov, too, found a constant rate during the reduction of UO_3 by methane in the composition range from $UO_{2.6} \rightarrow UO_{2.25}$. The reduction process, starting from UO_3, proceeds via the following phases: UO_3 U_3O_8 U_4O_9 UO_2. Of these the U_3O_8 lattice can contain a surplus or a deficit of oxygen and the UO_2 lattice can contain a surplus of oxygen up to $UO_{2.12}$. The conversion from U_3O_{8+x} to U_3O_{8-x} occurs in the presence of one solid phase. In the region between $UO_{2.6}$ and U_4O_9 two phases, each with a constant composition, are present. The final reduction to UO_2 occurs again in the presence of one phase. The existence of a composition range in which the rate depends little on the degree of reduction is ascribed by Vlasov to "the similarity of certain physical properties of the U_3O_{8-x} and U_4O_9 phases". We believe

that the constant reduction rate in region B is caused by the presence of two phases with different crystal structures. Therefore the number of degrees of freedom of the system is one less than in the single phase region A, resulting in a constant oxygen activity in the thermodynamic sense i.e. there is a constant oxygen pressure in equilibrium with the system. At the beginning of region C a similar behaviour would be expected. This is not found, possibly because U_4O_9 is an oxygen excess super lattice of UO_{2+x}, and therefore, as far as the oxygen activity is concerned, U_4O_9 and UO_{2+x} can be considered as one phase.

The different activation energies and reaction orders that we found for the reductions with hydrogen and ethylbenzene can only be explained when the oxygen diffusion is not the limiting step, an assumption that is also supported by data on the high mobility of oxygen in the lattices of uranium oxides, determined by isotopic exchange (10). The zero reaction order for ethylbenzene indicates that the active catalyst surface is almost completely occupied. Because the reduction rate for experiments with high hydrogen concentrations is faster than the highest ethylbenzene reduction rate, we may conclude that for the latter the chemical reaction is rate determining. The first order for hydrogen indicates that the chemisorption is probably rate determining in this case. De Marco (11), Morrow (12) and Dell (13) also observed that the kinetics of the hydrogen reduction of UO_3 were best interpreted in terms of hydrogen chemisorption as the rate controlling step.

3.5.2. REDUCTION OF CATALYST B

The results of the reduction of uranium oxide on alumina with hydrogen are shown in figures 3.11 and 3.12. The reaction conditions are the same as mentioned in

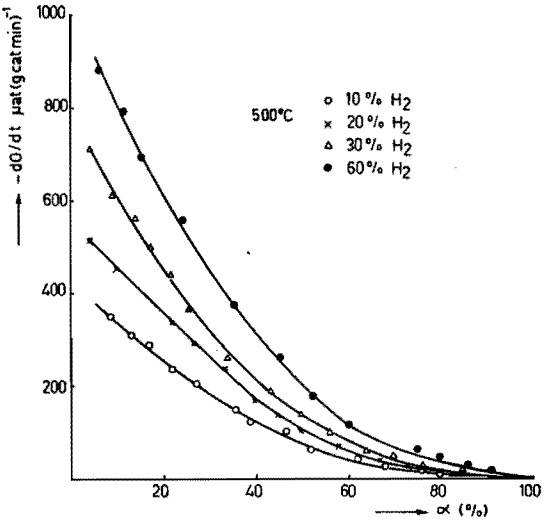

Fig. 3.11 Reduction rate as a function of the degree of reduction α at various hydrogen mole fractions; catalyst B.

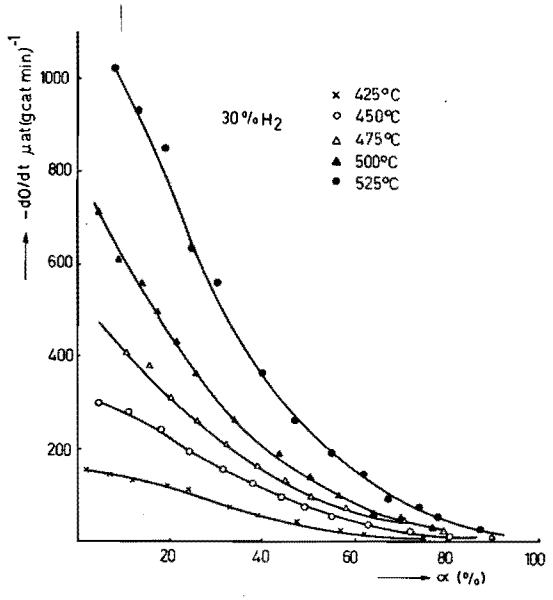

Fig. 3.12 Reduction rate as a function of the degree of reduction α at various temperatures; catalyst B, reduction with hydrogen.

table 3.3. The overall reduction behaviour of this catalyst is completely different from that of pure U_3O_{8+x}. None of the usually applied kinetic expressions for gas solid reactions - like for instance the "shrinking core" relation (14), product layer diffusion models applicable to reactions of the type A(gas) + B(solid) → P(gas) + Q(solid) (15,16) or models in which besides the reaction also oxygen diffusion through the lattice is incorporated - fitted the experimental data. Furthermore, a kinetic model involving different catalytic sites, as described recently by van Bokhoven (18) could not describe our experimental results.

Comparison of the hydrogen reduction curves of both catalyst A and B, shows that the average reduction rates, expressed in μat O (min gcat)$^{-1}$ are in the same range. Though catalyst B contains only 20 wt% uranium oxide, we may conclude that, in spite of the fact that the BET surface area is about 150 $m^2\ g^{-1}$, the active reduction surface area of this catalyst is about the same as of pure uranium oxide, and therefore should be also of the order of 6 $m^2\ g^{-1}$. This, then, is the uranium oxide surface area exposed to the gas phase if catalyst B is expected to consist of uranium oxide particles in an alumina matrix, as shown in figure 3.13. The continuous decrease in the reduction rate for catalyst B is, in our opinion, a result of a wide distribution of the relative size of the smaller crystallites. The rate of re-

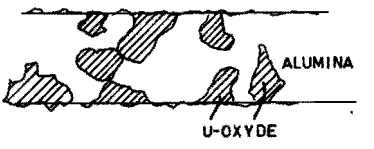

Fig. 3.13 Uranium oxide crystallites in alumina matrix.

duction of a pure uranium oxide particle with diameter d is given in figure 3.14. Assuming the reduction rate to be pro-

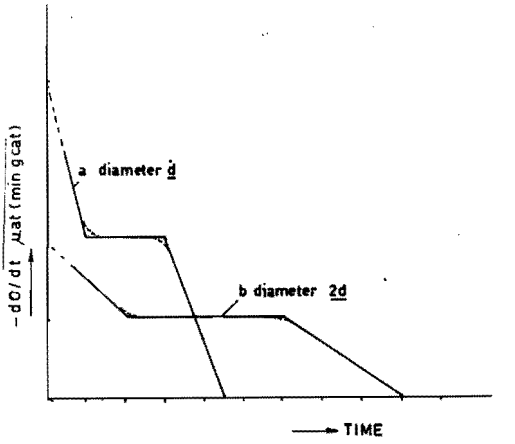

Fig. 3.14 Relation between reduction rate and crystallite size.

portional to the exposed surface, curve b for a particle with a particle diameter 2d can be easily derived from curve a. The average reduction rate of a catalyst, with a particle diameter distribution relatively wide in comparison to its average diameter, turns into a continuously decreasing curve. As the Al_2O_3 matrix will act as a barrier to the oxygen transport from one crystallite to the other, we feel that a description of catalyst B as a set of isolated uranium oxide crystallites in alumina is appropriate.

LITERATURE CHAPTER 3

1. Leroy, J.M., and Tridot, G., Compt. Rend. [C] 262, 114 (1966).
2. Cordfunke, E.H.P., "The Chemistry of Uranium". Elsevier Publishing Company, Amsterdam, 1969.
3. Cordfunke, E.H.P., J. Inorg. Nucl. Chem. 24, 303 (1962).
4. Heynen, H.W.G., and van der Baan, H.S., J. Catal.in press.
5. Steenhof de Jong, J.G., Guffens, C.H.E., and van der Baan, H.S., J. Catal. 26, 401 (1972).
6. Steenhof de Jong, J.G., Guffens, C.H.E., and van der Baan, H.S., J. Catal. 31, 149 (1973).
7. Notz, K.J., and Mendel, M.G., J. Inorg. Nucl. Chem. 14, 55 (1960).
8. Vlasov, V.G., and Semavin, Yu.N., J. Appl. Chem. USSR 40, 1169 (1967).
9. Vlasov, V.G., and Semavin, Yu.N., J. Appl. Chem. USSR 40, 374 (1967).
10. Johnston, E.J., Huttchison, A., and Katz, J.J., J. Inorg. Nucl. Chem. 7, 392 (1958).
11. De Marco, R.E., and Mendel, M.G., J. Phys. Chem. 64, 132 (1960).
12. Morrow, S.A., Graves, S., and Tomlinson, L., Trans. Faraday Soc. 57, 1400 (1961).
13. Dell, R.M.,and Wheeler, V.J., J. Phys. Chem. 64, 1590 (1960).
14. Levenspiel, O., "Chemical Reaction Engineering", Wiley, New York, 1962.
15. Massoth, F.E., and Scarpiello, D.A., J. Catal. 21, 225 (1971).
16. Seth, B.B.L., and Ross, H.U., Trans. Met. Soc. AIME 233, 180 (1965).
17. Batist, P.A., Kapteyns, C.J., Lippens, B.C., and Schuit, G.C.A., J. Catal. 7, 33 (1967).
18. Van Bokhoven, J.J.G.M., Thesis, Eindhoven, 1974.

CHAPTER 4

CHARACTERIZATION OF THE STIRRED REACTORS

4.1. INTRODUCTION

A stirred reactor behaves as a perfect mixer if the concentration and the temperature of the bulk gas phase are uniform. This is achieved by intensive mixing of the gas. A consequence is that the boundary layer round the particles is rather thin and therefore the mass transfer resistance is usually small. Because heat and mass transport occur by similar mechanisms, a reduction of mass transfer resistance implies that the temperature difference across the boundary layer decreases accordingly.

Every real reactor deviates to some degree from ideality. As long as this deviation is so small that its effects are well within the range of experimental error, the reactor can be treated as an ideal reactor for all practical purposes. Noticeable, but still minor deviations from ideality can be treated with the aid of simple approximations.

Below we describe experiments and calculations performed in order to find out how far our reactors deviate from ideality.

4.2. MIXING OF THE GAS PHASE

Different methods are described in the literature to judge the degree of mixing in a stirred gas solid reactor. Trotter (1) studied the kinetics of a simple first order reaction, the true kinetics of which were known; other authors measured conversions at different stirrer speeds (2,3,4,5,6) or used tracer techniques (7,8,9,10). We have

used styrene productivity measurements and tracer experiments; moreover, we were able to determine the actual gas flow through the catalyst bed by pressure drop measurements. This method was also applied by Berty (11).

To characterize reactor A, residence time distribution functions $F(\tau)$ were determined for various feed rates and stirring speeds varying from 0 - 6600 rpm. If the reactor is perfectly mixed, the response to a step function is described by:

$$F(\tau) = 1 - e^{-t/\tau} = conc/conc_o$$

with conc = outlet concentration
$conc_o$ = inlet concentration
τ = mean residence time in the reactor
= free volume of the reactor / feed rate.

The step was created by switching from a steady flow of nitrogen to a steady flow of oxygen or vice versa. The flow diagram of the system is shown in figure 4.1. The step

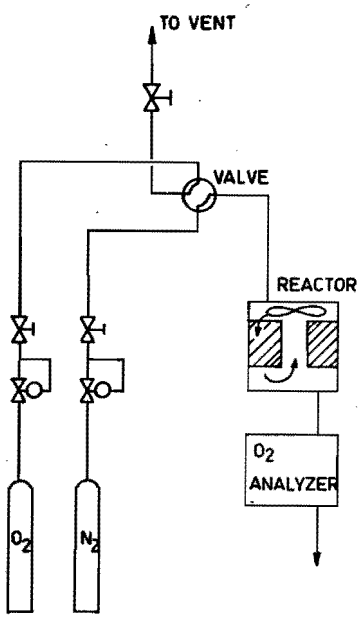

Fig. 4.1 Flow diagram for step response measurements.

changes are generated with the aid of a Becker valve. The resistance of the vent is adjusted so that there is no change in flow rate when the valve is turned. The connecting tubes between valve, reactor and Servomex oxygen analyzer have an internal diameter of 1/32 inch and were kept as short as possible.

The $F(\tau)$ curves were determined at the same pressure, temperature and flow conditions as during the chemical experiments. The reactor characteristics $\ln(1 - \text{conc}/\text{conc}_o)$ versus t/τ at feed rate 4.4 l h^{-1} NTP and four stirring speeds are given in figure 4.2. From the experiment at

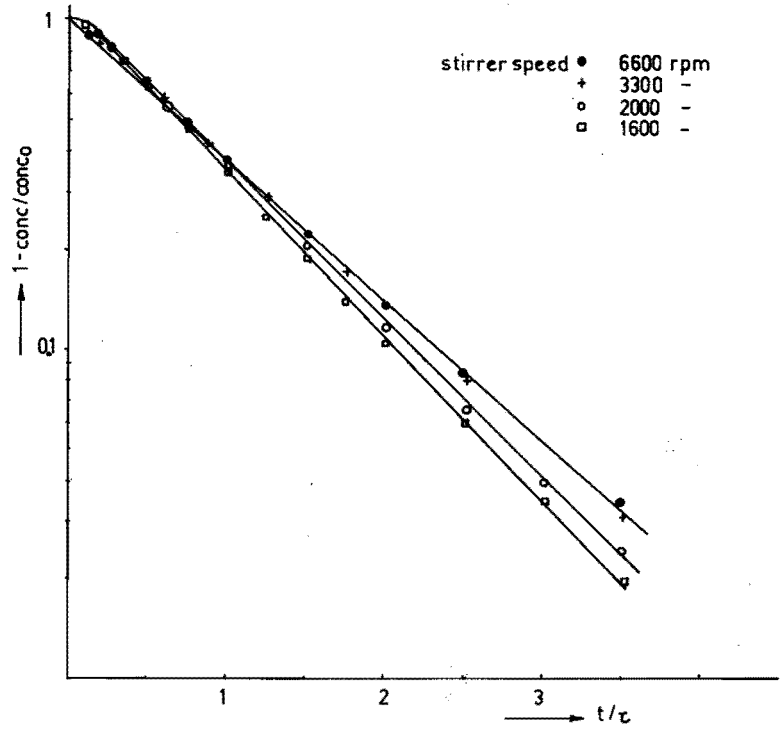

Fig. 4.2 CSGSR responses to a step function at various stirrer speeds: catalyst holder A filled with 360 g of siliconcarbide (1 - 1.4 mm); nitrogen or oxygen feed rate 4.4 l h^{-1} NTP; temperature 500°C.

6600 rpm a τ-value of 113 sec was determined, which is in good agreement with the value of 115 sec expected from the free reactor volume of 404 cm^3. In this case we have chosen as a criterion for ideal mixing that the maximum deviation between the actual step response curve and the ideal one is less than 2%. The deviations are plotted versus t/τ in figure 4.3, from which we conclude that the reactor is perfectly mixed when the stirring speed is higher than

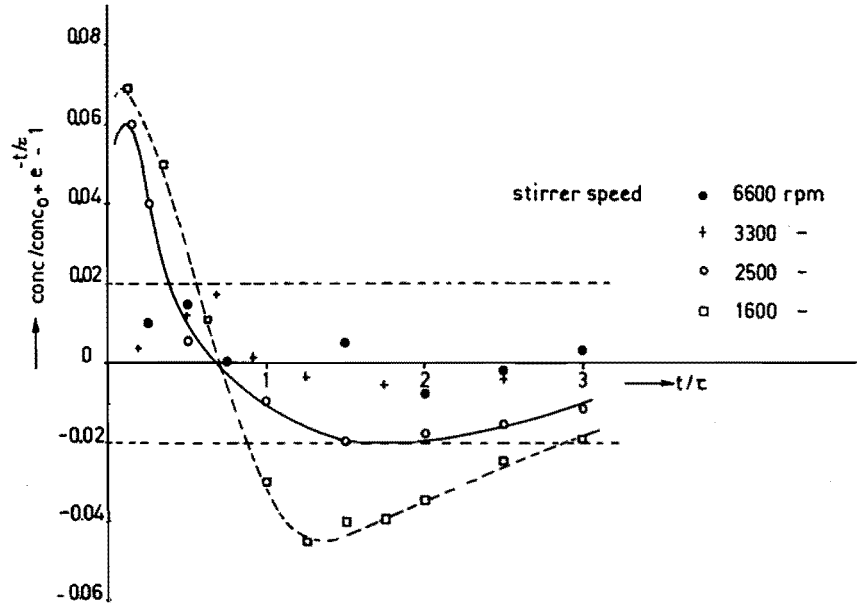

Fig. 4.3 Deviation of the step response of reactor A from that of an ideal mixer versus t/τ: conditions of figure 4.2.

3300 rpm. For higher feed rates, higher speeds are needed to meet the mixing criterion.

Another criterion that can be used to characterize the mixing is that the concentration gradient across the catalyst bed is less than say 2%. This definition is convenient when the mixer is visualized as a recirculated plug flow

Table 4.1 Recirculation number n required to satisfy the mixing criterion: $(c_i - c_{out})/c_i < 0.02$.

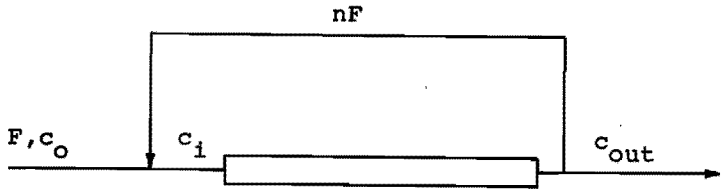

outside feed conversion	recirculation number
$1-c_{out}/c_o$	n
0.9	440
0.8	195
0.7	114
0.6	73
0.5	48
0.4	32
0.3	20
0.2	12
0.1	5
0.05	2

reactor, with n recirculations (see table 4.1). The actual recirculation number was calculated from pressure drop measurements over the catalyst bed with the Ergun relation (12). With this relation first the actual porosity of the catalyst bed was calculated from measurements of the pressure drop as a function of the outside feed rate through the plug flow reactor (central hole of the catalyst holder closed). The number of internal recirculations n of the CSGSR is defined as:

$$n = \frac{\text{gas flow through the bed} \quad (1\ h^{-1})}{\text{reactor gas feed} \quad (1\ h^{-1})} - 1 \qquad (4.1)$$

In figure 4.4 for reactor A the pressure drop over the catalyst bed (=pressure head of the fan) and n are given as a function of the stirrer speed. The internal recirculation number n is high for this reactor because the denominator of equation 4.1 is very small i.e. the outside feed (4.6 - 18.5 1 h^{-1}NTP) causes a very low linear gas velocity in the bed, having a cross sectional area of 44.5 cm^2. This makes it impossible to use the catalyst holder A for plug flow experiments, because almost complete back mixing ($D_a/uL \approx 1$ (13)) will occur. Therefore reactor B was constructed, which behaved as a good plug flow reactor (D_a/uL= 0.03 - 0.008), because the linear gas velocity caused by the outside gas feed was much higher than for reactor A,

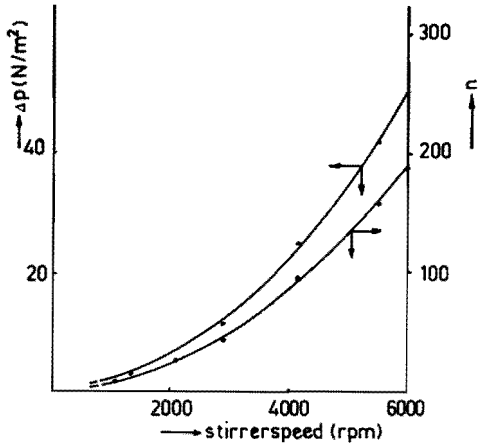

Fig.4.4 Internal recirculation number n and pressure drop over the catalyst bed versus stirrer speed: catalyst holder A filled with 360 g of silicon-carbide (1 - 1.4 mm); cross sectional area catalyst bed 44.5 cm^2; nitrogen feed rate 4.4 1 h^{-1} NTP; temperature 500°C.

the cross sectional area of the catalyst bed being only 3.1 cm^2. But this small bed cross-section resulted in a high pressure drop during mixer experiments. In order to provide still enough recirculations at high outside feed rates, the following measures were taken:

- the maximum stirrer speed was increased from 6600 to 10,000 rpm,
- a volute construction (figure 2.4) was applied for catalyst holder B,
- instead of nitrogen, a heavier gas, viz. carbondioxide, was used.

In figure 4.5 the recirculation number n and the pressure

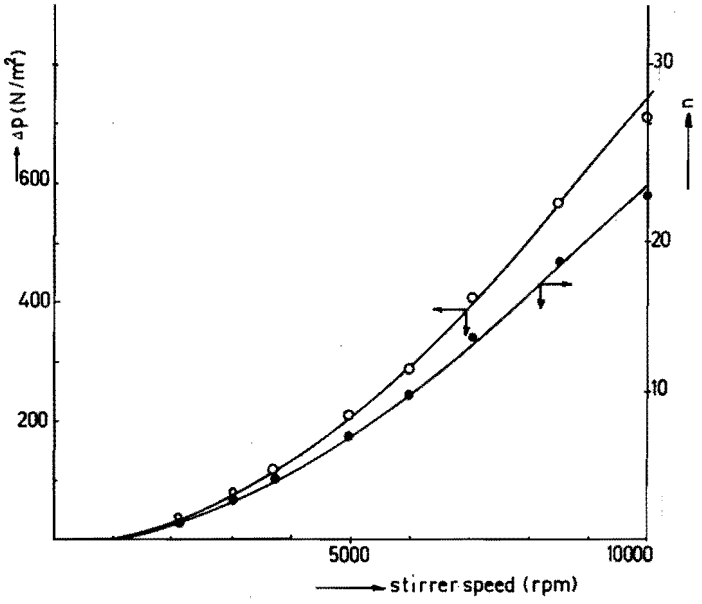

Fig. 4.5 Internal recirculation number n and pressure drop over the catalyst bed versus stirrer speed: catalyst holder B filled with 8.0 g of uranium oxide on alumina (0.6 - 1.0 mm); cross sectional area catalyst bed 3.1 cm^2; carbondioxide feed rate 4.4 l h^{-1} NTP; temperature 500°C.

drop over the bed as a function of the stirrer speed are given for reactor B. Reactor A approaches ideal mixing better than B, but as we wanted to do both mixing and plug flow experiments in one reactor, a compromise in regard to the deviation from ideality of mixer and plug flow reactor had to be accepted. To compare the two mixing criteria, the average step response of a recirculated plug flow reactor with n recirculations (see table 4.1) is represented in figure 4.6. It can be shown that especially at low t/τ the plug flow reactor response deviates from the ideal mixer response, About 24 recirculations are needed to keep the maximum deviation from ideal mixing below 2%.

Mixing in the catalyst bed of reactor B could not be assessed accurately by the step response method because the volume of the catalyst bed is much smaller than the total free volume of the reactor.

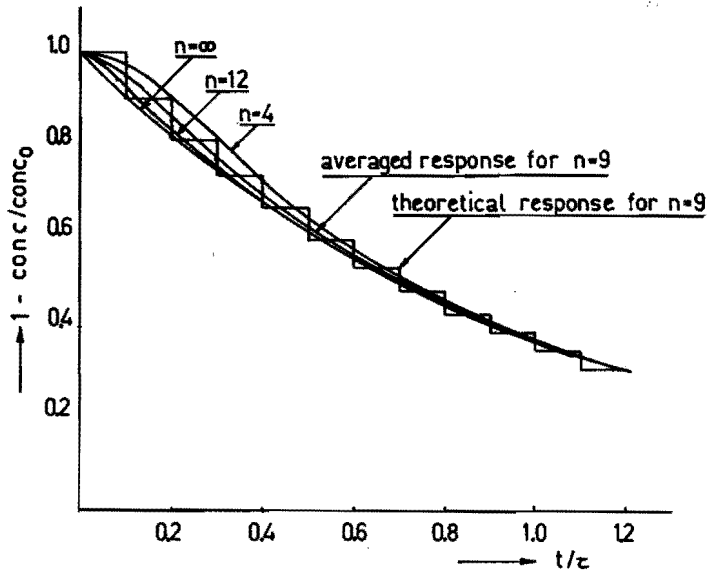

Fig. 4.6 Response of recirculated plug flow reactor to a step function.

In figure 4.7 it is shown that the styrene production as a function of the stirrer speed passes through a maximum and tends to remain constant above stirrer speeds of about 6000 rpm for a reactor feed gas stream of 4.6 l h^{-1} NTP. For the highest feed rate 18.5 l h^{-1} NTP a speed of 8000 rpm is required to approach this condition. At very low n the styrene production is low because by-passing through the central hole occurs, while at intermediate n the reactor behaves as a plug flow reactor with a low number of recirculations.

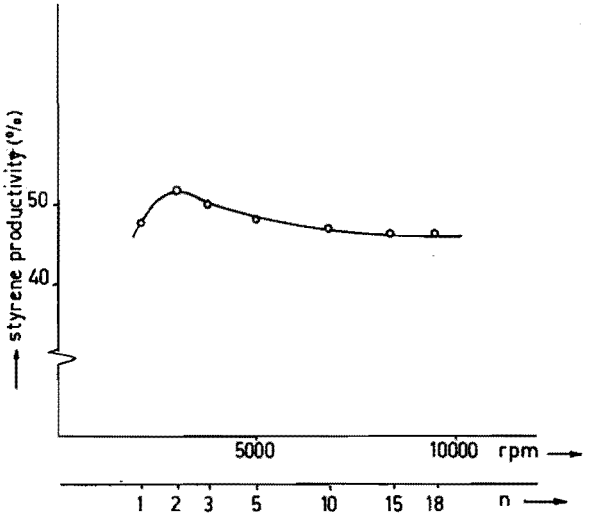

Fig. 4.7 Styrene productivity versus stirrer speed and corresponding internal recirculation number n: catalyst holder B filled with 8.0 g of uranium oxide on alumina (0.6 - 1.0 mm); gas flow rate 4.6 l h^{-1} NTP carbondioxide; ethylbenzene vapour pressure 20 mm Hg.

The experimental data obtained in reactor B were corrected for the non-ideality of mixing and plug flow, as will be shown in chapter 5. Therefore, the mixer was described as a recirculation reactor with n recirculations and the plug flow reactor as an ideal one with axial dispersion (13).

4.3. MASS AND HEAT TRANSFER BETWEEN GAS AND CATALYST SURFACE

Above stirrer speeds of about 7000 rpm the productivity in the CSGSR B remains constant, as shown in §4.2. From this we may conclude that the resistance to mass transfer to the catalyst surface is negligible under these conditions. Heat and mass transfer coefficients were also calculated for a plug flow experiment carried out under the following conditions: temperature 495^{o}C, ethylbenzene vapour pressure 3 mm Hg, carbondioxide feed rate 4.6 l h^{-1} NTP, 8 g catalyst B, conversion reached 80%. The calculations were carried out according to Satterfield and Sherwood (14) and Hougen (15) with data of Appendix II. The calculated ratio of the concentration drop across the boundary layer and the average bulk concentration was 0.003 and the temperature drop was about 0.01^{o}C. These calculations show that under the conditions used for the kinetic experiments (see table 5.1) no transport limitations between gas phase and catalyst surface have to be expected.

LITERATURE CHAPTER 4

1. Trotter, I.P., Ph.D. Thesis, Princeton University, 1960.
2. Ford, F.E., Perlmutter, D.D., Chem. Eng. Sci. 19, 371 (1964).
3. Lakshmanan, R., Roulean, D., Can. J. Chem. Eng. 47, 45 (1969).
4. Lakshmanan, R., Roulean, D., J. Appl. Chem. 20, 312 (1970).
5. Brown, C.E., Bennett, C.O., AIChE J. 16, 817 (1970).
6. Livbjerg, H., and Villadsen, J., Chem. Eng. Sci. 26, 1495 (1971).
7. Carberry , J.J., Ind. Eng. Chem. 56 (11), 39 (1964).
8. Tajbl, D.G., Feldkirchner, H.L., Lee, A.L., Advan. Chem. Ser. 69, 166 (1967).
9. Brisk, M.L., Day, R.L., Jones, M., Warren, J.B., Trans. Inst. Chem. Eng. 46 (1), T(3) (1968).
10. Bennett, C.O., Cutlip, M.B., and Yang, C.C., Chem. Eng. Sci. 27, 2255 (1972).
11. Berty, J.M., Hambrick, J.O., Malone, T.R., and Ullock, D.S., AIChE Meeting, New Orleans, La. 1969.
12. Ergun, S., Chem. Eng. Progr. 48, 89 (1952).
13. Levenspiel, O., "Chemical Reaction Engineering", John Wiley and Sons, Inc., New York, London, 1962.
14. Satterfield, C.N., and Sherwood, T.H., "The role of diffusion in catalysis", Addison-Wesley Publishing Company, Reading (Mass.) 1963.
15. Hougen, O.A., Ind. Eng. Chem. 53, 509 (1961).

CHAPTER 5

REACTION KINETICS

5.1. PRELIMINARY EXPERIMENTS

Before the evaluation of kinetic models of solid catalyzed reactions is undertaken, the following possible sources of error should be investigated:

- changes in the catalyst activity
- bulk phase mass and heat transfer resistance
- non-unity effectiveness factors
- non-ideality of reactor flow pattern.

In the previous chapter it was shown that external mass and heat transfer limitations can be neglected and that only slight corrections have to be applied to the non-ideality of the reactors.

Most of the preliminary experiments were carried out in the plug flow reactor of figure 2.2. If not stated otherwise, all experiments were carried out with the same batch of catalyst B (Uranium oxide on alumina).

A 160-hour experiment under conditions similar to those of the kinetic experiments showed that no decrease in catalyst activity occurs.

Tests for absence of pore diffusion limitation were done by increasing the average catalyst diameter fourfold. The results of these experiments, given in figure 5.1, show that the conversion is not affected by the catalyst diameter and consequently for these particle diameters pore diffusion can be neglected. Calculation of effectiveness factors according to Satterfield and Sherwood (1) have also established that under the experimental conditions these factors hardly deviate from unity. The data used for this calculation are given in Appendix II.

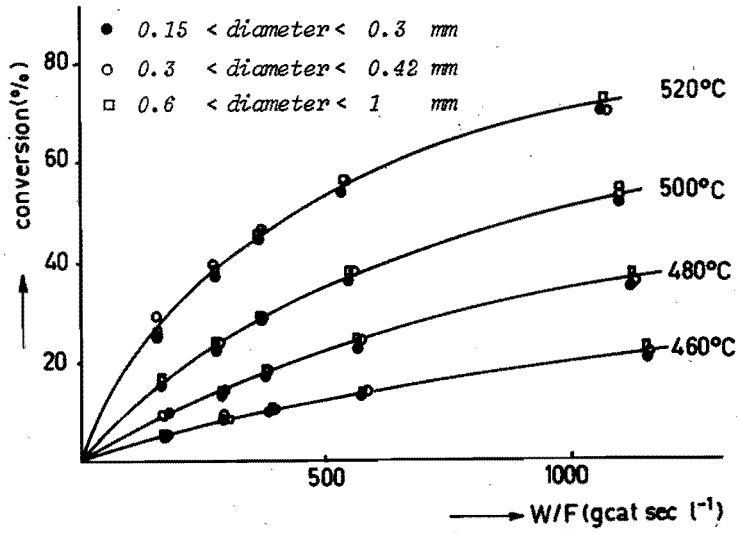

Fig. 5.1 Ethylbenzene conversion versus W/F at various catalyst diameters: plug flow fixed bed reactor filled with 2.0 g of catalyst B; carrier gas nitrogen; ethylbenzene vapour pressure 7.3 mm Hg.

That the conversion of ethylbenzene only depends on the time of contact with the catalyst, in other words, that, if the amount of catalyst or the feed rate is varied, equal W/F-values (W = amount of catalyst, F = gas flow rate under reaction conditions) give equal conversions, is shown in figure 5.2.

From these data it follows that at constant W/F a variation of the amount of catalyst or dilution of the catalyst with siliconcarbide has no effect on the conversion. Moreover, experiments at 500°C with an ethylbenzene vapour pressure of 3 mm Hg, which is the lowest applied during the kinetic study, showed that at feed rates above 2.5 l h^{-1} NTP the conversion in the empty stainless steel plug flow and the mixed reactors is less than 1%. The same results were obtained when the reactors were filled with siliconcarbide (0.6 - 1 mm), which was sometimes used as a catalyst diluent.

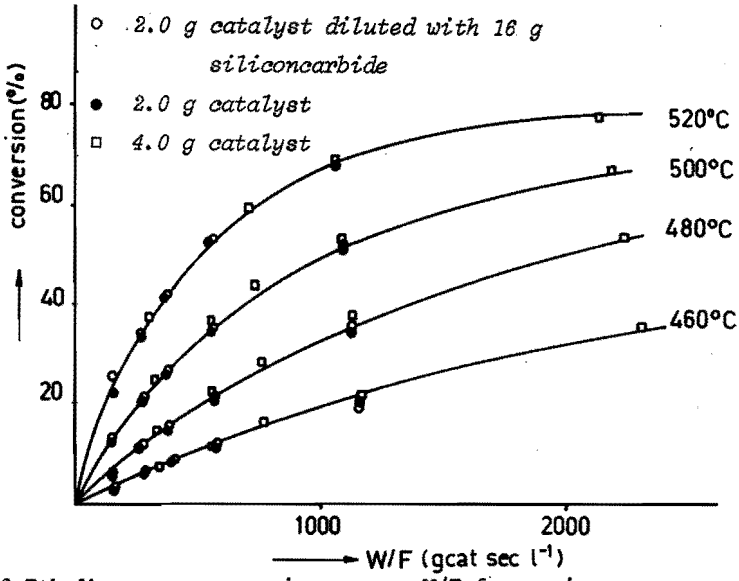

Fig. 5.2 Ethylbenzene conversion versus W/F for various amounts of catalyst: plug flow fixed bed reactor filled with catalyst B (0.15 - 0.30 mm); carrier gas nitrogen; ethylbenzene vapour pressure 7.3 mm Hg.

From the above it follows that either adsorption of ethylbenzene or the chemical reaction at the catalyst surface or desorption of products is rate controlling. We imagine that in the reaction step an adsorbed ethylbenzene molecule loses hydrogen, leaving an adsorbed styrene molecule on the surface, which will desorb subsequently. As far as the hydrogen is concerned several pathways are open:

a. hydrogen adsorption is competitive with ethylbenzene and styrene adsorption, in other words, the two sites required for hydrogen and hydrocarbon adsorption are identical and interchangeable and do not belong together in any specific way.
b. hydrogen and styrene adsorb on one complex (kinetic) site; this site may very well consist of a number of reactive subsites.

c. only the hydrocarbon is adsorbed on the catalyst and the hydrogen is liberated as such to the gas phase.

If the chemical reaction is supposed to be rate determining, the pathways a, b and c lead to the following rate equations respectively:

$$-\frac{dc}{dW/F} = \frac{k(c - c_{St}c_H/k_{eq})}{(1 + KEc + KSc_{St} + KHc_H)^2} \qquad (5.1)$$

$$-\frac{dc}{dW/F} = \frac{k(c - c_{St}c_H/k_{eq})}{1 + KEc + KSc_{St} + KSKHc_{St}c_H} \qquad (5.2)$$

$$-\frac{dc}{dW/F} = \frac{k(c - c_{St}c_H/k_{eq})}{1 + KEc + KSc_{St}} \qquad (5.3)$$

Because of the high reaction temperatures the adsorption constant of hydrogen (and of carrier gas) should be considerably lower than the corresponding constants for hydrocarbons and are therefore omitted in the rate equation. Consequently, no distinction can be made between the reaction routes b and c (unless extremely large variations of the hydrogen concentration are applied).

If equation 5.1 applies, then for differential conversion levels a linear relation exists between $(c_o/r)^{\frac{1}{2}}$ and c_o, while $1/r$ versus $1/c_o$ gives a straight line if equation 5.3 applies.

We carried out such differential experiments in a glass plug flow reactor with a small amount of catalyst. The results of these experiments are plotted in figures 5.3 and 5.4, from which it follows that equation 5.3 can describe the data. These experiments, however, were done with

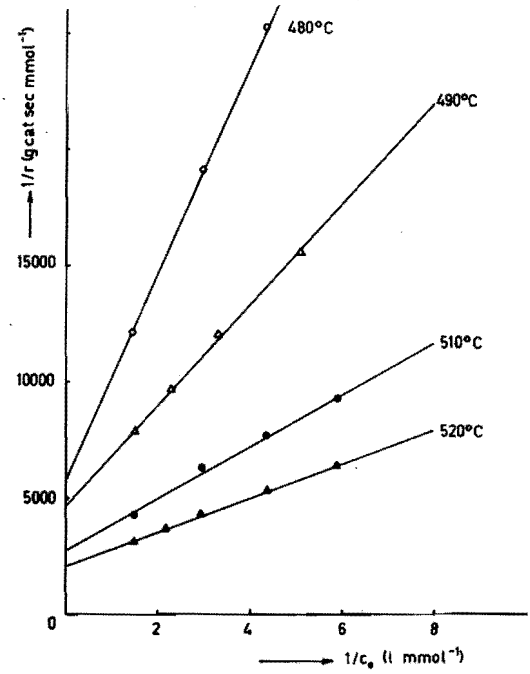

Fig. 5.3 Differential measurements, $1/r$ versus $1/c_o$: plug flow fixed bed reactor filled with 0.2 g of catalyst B (0.15 - 0.30 mm); carrier gas nitrogen.

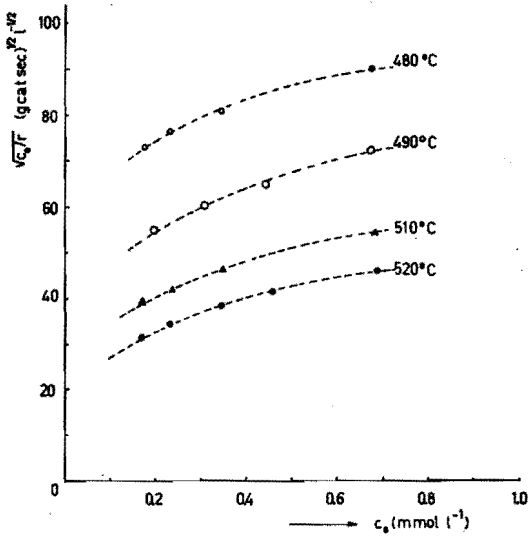

Fig. 5.4 Differential measurements, $\sqrt{c_o/r}$ versus c_o: conditions of figure 5.3.

a catalyst from a batch that has not been used in our further studies. Therefore, the kinetic constants that can be obtained from figure 5.3 have not been taken into account in this study, although they are comparable to those obtained later on.

Since no appreciable amounts of by-products were found, (the selectivities for styrene varied from 95-98%) equation 5.3 changes to:

$$\frac{dc_{St}}{dW/F} = \frac{k(c_o - c_{St} - c_{St}c_H/k_{eq})}{1 + KE(c_o - c_{St}) + KSc_{St}} \qquad (5.4)$$

The equilibrium constant k_{eq} was calculated from data given by Boundy (2).

5.2. EXPERIMENTAL PROCEDURE

The kinetic experiments were carried out in CSGSR B under both mixing and plug flow conditions, at five different initial concentrations, each at three temperature levels and four flow rates, as shown in table 5.1. The measuring procedure was as follows. The reactor was heated to reaction temperature and the desired ethylbenzene vapour pressure was established. At each temperature the sequence of the vapour pressures was random, and at each selected temperature and vapour pressure, the carrier gas feeds were again adjusted in arbitrary sequence. When the composition of the outlet gas did not change anymore, the reactor could be switched over to the other mode of operation, without necessity of any adjustment of reaction conditions.

Since we knew from preliminary experiments with pure UO_2 as catalyst (3) that the styrene adsorption constant KS could vary by a factor 2 to 5 without appreciably influencing the sum of squares of the differences of the observed and the calculated concentrations of equation 5.9, we also

Table 5.1 Reaction conditions for kinetic experiments in both fixed bed and CSGSR.

reaction temperature	vapour pressure in feed gas		feed gas flow
^{o}C	mm Hg		1 h^{-1} NTP
	ethylbenzene	styrene	
465	3.0	0	5
	7.5	0	7.5
480	8.55	6.1	10
495	14.0	0	20
	30.3	0	

Feed gas: carbondioxide, purity 99.995%
Catalyst: 8.00 g, 20 wt% UO_2 on Al_2O_3, 0.6-1 mm
Stirrer speeds during CSGSR experiments:
From 8,000 rpm at feed gas flow 5 1 h^{-1} NTP to
10,000 rpm at feed 20 1 h^{-1} NTP

did the experiments with a feed containing 8.55 mm Hg ethylbenzene and 6.1 mm Hg styrene in order to narrow down the value for KS. These experiments were only carried out under plug flow conditions. In order to prevent a noticeable change in the composition of the ethylbenzene styrene gas feed mixture, the contents of vaporizer V_2 was renewed after each experiment.

Moreover, we also applied a differential method to determine KS directly. Nitrogen containing 1.2 mol % of hydrogen was led through vaporizer V_2 filled with styrene (plus "ionox 100" as polymerization inhibitor). This mixture was passed through the differential glass reactor, filled with 0.5 g of the catalyst used in CSGSR B for the

measurements described above. A maximum conversion of about 2.7% was allowed during the ethylbenzene formation rate measurements as a function of the styrene feed concentration.

5.3. PROCEDURE FOR CALCULATING THE KINETIC PARAMETERS

For experiments with nitrogen as a carrier gas the amounts of styrene and hydrogen detected in the ethylbenzene dehydrogenation products are almost equal. However, as explained in section 4.2, carbondioxide was used as a carrier gas in the latter kinetic experiments, and then the amounts of styrene and hydrogen are no longer equal, as the hydrogen reacts with the carbondioxide. This means that for the integration of equation 5.4 an additional expression for c_H is required. It was found that for both plug flow and mixing experiments at each reaction temperature the c_H/c_o ratio could be described by an empirical relation of the form:

$$c_H/c_o = A\ W/F + B\ (W/F)^2 \qquad (5.5)$$

with a standard deviation below 0.01. We have not gone further into this matter since the empirical equation was sufficiently accurate for our purpose, i.e. the study of the kinetics of the dehydrogenation reaction.

For the plug flow reactor the concentration c_{St} at the outlet was calculated numerically by the Runge Kutta method, as a function of W/F, c_o, c_{Sto}, k, KE and KS, and the appropriate values for A and B, with:

$$\frac{dc_{St}}{dW/F} = \frac{k\{c_o+c_{Sto}-c_{St}-c_{St}c_o\,(A\ W/F + B(W/F)^2)/k_{eq}\}}{1 + KE(c_o + c_{Sto} - c_{St}) + KS\ c_{St}} \qquad (5.6)$$

For the CSGSR a mass balance yields:

$$rW = F\, c_{St} \tag{5.7}$$

(No CSGSR experiments with styrene in the feed gas were carried out).

$$\frac{W}{F} = \frac{c_{St}\left\{1 + KE(c_o - c_{St}) + KS\, c_{St}\right\}}{k(c_o - c_{St} - c_{St}c_H / k_{eq})}$$

$$= \frac{c_{St}\left\{1 + KE(c_o - c_{St}) + KS\, c_{St}\right\}}{k\left\{c_o - c_{St} - c_{St}c_o\,(A\, W/F + B(W/F)^2)/ k_{eq}\right\}} \tag{5.8}$$

From this equation the outlet concentration c_{St} could be solved directly as a function of W/F, c_o, k, KE and KS. If the relations 5.6 and 5.8 are adequate for the description of the integral experiments, the unknown parameters k, KE and KS are at one reaction temperature constant for all experiments in both reactor types. The best estimates of the parameters have been determined by searching for that set of parameters that gave the lowest sum of squares:

$$\sum_{j=1}^{n} \left[\frac{(c_{St,j})_{theor} - c_{St,j}}{c_{o,j}}\right]^2 \tag{5.9}$$

or:

$$SS = SS\,(\hat{k}, \hat{KE}, \hat{KS}_{int})$$

$$= \sum_{j=1}^{n} \left[\frac{(c_{St,j}\,(\hat{k}, \hat{KE}, \hat{KS}_{int}))_{theor} - c_{St,j}}{c_{o,j}}\right]^2 \tag{5.10}$$

with:

$(c_{St,j})_{theor}$ = styrene reactor outlet concentration calculated with relation 5.6 or 5.8.

SS = the residual sum of squares of the deviations between the calculated and the observed styrene productivities.

n = number of observations at one reaction temperature.

$\hat{k}$, $\hat{KE}$, $\hat{KS}_{int}$ = estimators of k, KE and KS that minimize relation 5.9.
For convenience, we shall in this chapter distinguish between $\hat{KS}_{int}$, the value for KS estimated from the integral experiments and the estimator $\hat{KS}_{dif}$ calculated from differential data.

The non-linear optimization problem was solved with an Algol 60 computer program, which was derived from a general procedure, described by Lootsma (4), that can be used for solving constrained or unconstrained minimization problems and is based on the Broyden, Fletcher, Shanno algorithm (5, 6,7).

The differential experiments, starting from styrene and hydrogen provided ethylbenzene formation rates as a function of the styrene feed concentrations. From these data, estimates for KS were calculated as follows:
Under differential conditions equation 5.4 changes to

$$r = \frac{\Delta c_{EB}}{\Delta W/F} = \frac{k\, c_{Sto}\, c_{Ho} / k_{eq}}{1 + KS\, c_{Sto}} \qquad (5.11)$$

or

$$\frac{1}{r} = \frac{1}{k\, c_{Ho} / k_{eq}} \frac{1}{c_{Sto}} + \frac{KS}{k\, c_{Ho} / k_{eq}} \qquad (5.12)$$

$$= \frac{\beta_1}{c_{Sto}} + \beta_o \qquad (5.13)$$

From a plot of $1/r$ versus $1/c_{Sto}$ (figure 5.5) is found:

$$\hat{KS}_{dif} = \hat{\beta}_o \; / \; \hat{\beta}_1 \qquad (5.14)$$

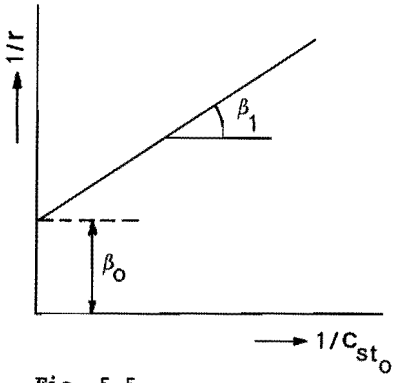

Fig. 5.5

5.4. *EXPERIMENTAL RESULTS AND CORRECTIONS FOR NON-IDEAL REACTOR BEHAVIOUR*

The results of the differential measurements at 495, 480 and 465°C are given in table III.4 (Appendix III). The best straight lines through the data points are shown in figure 5.6. This resulted in the values for the constants $\hat{\beta}_o$ and $\hat{\beta}_1$ of equation 5.14 and in the $\hat{K}S_{dif}$ values detailed in table 5.2.

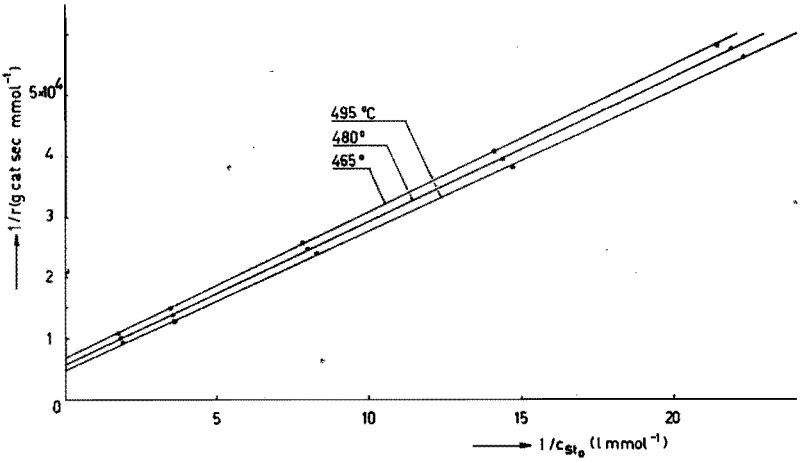

Fig. 5.6 Differential ethylbenzene formation measurements starting from styrene and hydrogen, 1/r versus $1/c_o$: conditions of table III.4.

The experimental results obtained in reactor B under both plug flow and mixing conditions are given in tables III.1, III.2 and III.3. From the observed hydrogen concentrations the parameters A and B of equation 5.5 were calculated by least squares fitting; the values obtained for A and B are given in table 5.3. As an example, the close agreement between observed and calculated c_H is demon-

Table 5.2 Styrene adsorption constants $\hat{K}S_{dif}$ from differential measurements.

temp.	$\hat{\beta}_o$	$\hat{\beta}_1$	$\hat{K}S_{dif} = \hat{\beta}_o/\hat{\beta}_1$
°C	sec g cat $mmol^{-1}$	sec g cat l^{-1}	l $mmol^{-1}$
495	0.476	0.230	2.07
480	0.562	0.237	2.38
465	0.657	0.242	2.72

Table 5.3 A and B values of equation 5.5 calculated with observed hydrogen concentrations.

temp.	A	B
°C	l $(g\ cat\ sec)^{-1}$	l^2 $(g\ cat\ sec)^{-2}$
	plug flow	
495	1.58×10^{-4}	-3.33×10^{-8}
480	1.41×10^{-4}	-3.03×10^{-8}
465	1.08×10^{-4}	-2.02×10^{-8}
	mixer	
495	1.33×10^{-4}	-2.88×10^{-8}
480	1.19×10^{-4}	-2.30×10^{-8}
465	0.94×10^{-4}	-1.72×10^{-8}

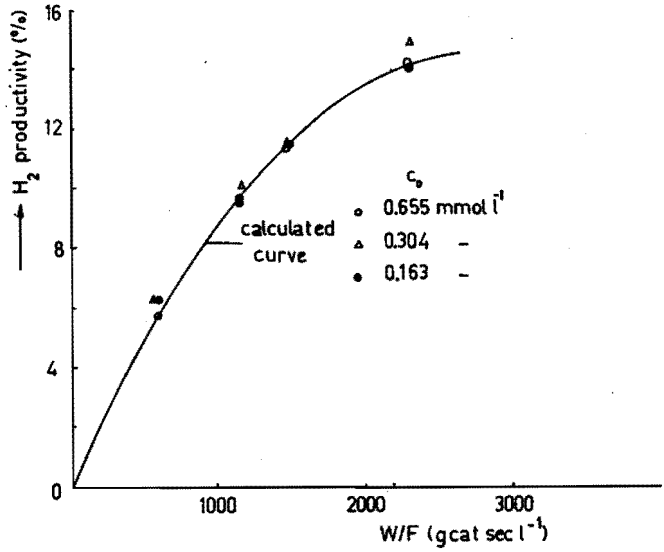

Fig. 5.7 Observed and calculated hydrogen concentrations versus W/F under plug flow conditions at 465°C.

strated in figure 5.7 for the plug flow experiments at 465°C. With the observed styrene productivity data for the plug flow experiments of tables III.1, III.2 and III.3 and the $\hat{K}S_{dif}$ values of table 5.3, $\hat{k}$ and $\hat{K}E$ were calculated with the search program as explained in section 5.3. The resulting parameter estimates and the total sum of squares (j = 1 to 20) for the plug flow experiments are given in table 5.4. For instance, the curves for the experiments at 495°C were calculated with these parameters for both plug flow and stirred reactor conditions. This is shown in figures 5.8 and 5.9. From the latter figure it can be seen that the observed styrene productivities for the stirred reactor are a little higher than those predicted from the plug flow experiments. One reason for these deviations is that both the plug flow and the stirred reactor are not ideal. This tends to bring the experimental conversion curves for both reactor types nearer to each other, as

Table 5.4 Kinetic constants calculated with observed styrene productivities of the plug flow experiments.

temp.	$\hat{k}$	$\hat{K}E$	SS*	$\hat{K}S_{dif}$	k_{eq}
°C	$l(g\ cat\ sec)^{-1}$	$l\ mmol^{-1}$		$l\ mmol^{-1}$	$mmol\ l^{-1}$
495	6.99×10^{-4}	1.94	5.7×10^{-3}	2.1	0.343
480	5.22×10^{-4}	1.76	2.6×10^{-3}	2.4	0.237
465	3.88×10^{-4}	1.77	4.4×10^{-3}	2.7	0.162

* j = 1 to 20

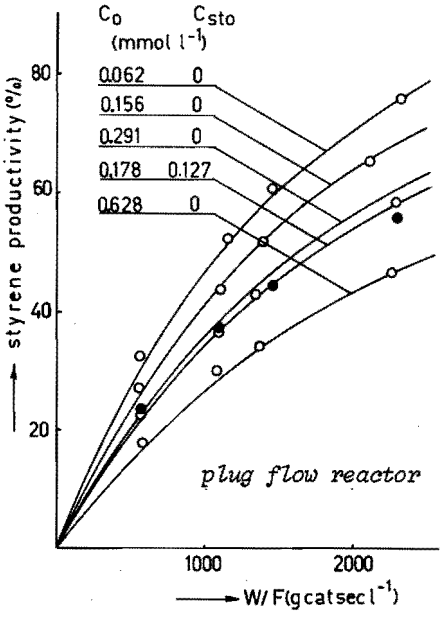

Fig. 5.8

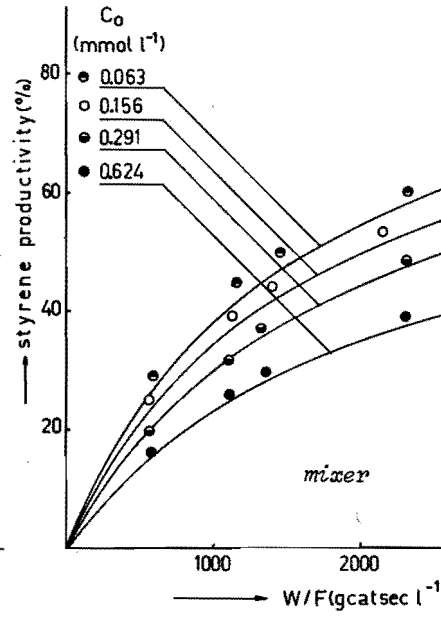

Fig. 5.9

Observed styrene productivities versus W/F: temperature 495°C. Curves calculated with parameter estimates of table 5.4.

would have been the case if both reactors had behaved ideally. Therefore, the systematic errors introduced by using the formulae for ideal reactors were corrected as follows.

The fluid flow in the actual plug flow reactor is considered to be ideal plug flow on which is superimposed some axial mixing. This axial mixing or axial dispersion is characterized by the dimensionless group D_a/uL, which usually represents quite satisfactorily flow that does not deviate much from plug flow. The axial dispersion coefficient D_a can be taken equal to the molecular diffusion coefficient D under the plug flow experimental conditions, because in all cases the Reynolds number was smaller than 0.5 (8,9). The differential equation describing the effect of axial dispersion on the chemical reaction can only be solved analytically for simple kinetics; in most other cases numerical solution procedures are required. However, for slight deviations from plug flow Pasquon (10) derived the equation:

$$c_A - c_{Ap} = D/uL \; r_{Ap} \; W/F \; \ln (r_{Ap} / r_{Apo}) \qquad (5.15)$$

where r_{Apo} and r_{Ap} are the rates at the inlet and the outlet of an ideal plug flow reactor of the same W/F as the real one and $c_A - c_{Ap}$ is the concentration difference between the real and the ideal reactor. With equation 5.15, which holds for any kinetics, and the parameters of table 5.4, the styrene productivities for the plug flow experiments of the tables III.1, III.2 and III.3 (Appendix III) were corrected. In these tables the D/uL numbers used are given as well. The deviation from ideality of the mixer experiments were taken care of by visualizing the CSGSR as a recirculated plug flow reactor as described in section 4.2. The conversion in a reactor with an infinite number of recirculations is equal to that of an ideal mixer. As the recirculation number in the actual reactor was known, the

difference in conversion between the recirculation and an ideal mixed reactor could be calculated with the parameters of table 5.4. The results of this correction, which had to be carried out numerically, and the recirculation numbers n, are shown in the tables III.1,III.2 and III.3. With the corrected styrene productivity data of the plug flow and the mixer experiments together (j = 1 to 36), estimates for k, KE and KS were calculated again. As shown in figures 5.10 to 5.15 the corrected productivity data, both for the plug flow reactor and the CSGSR, fitted well on the curves calculated with the parameter estimates of table 5.5.

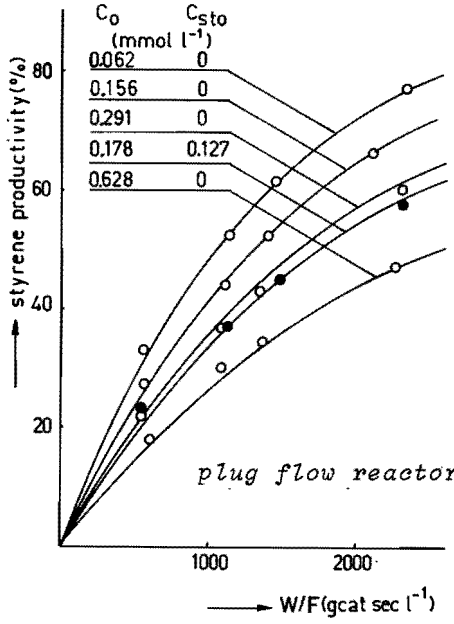

Fig. 5.10

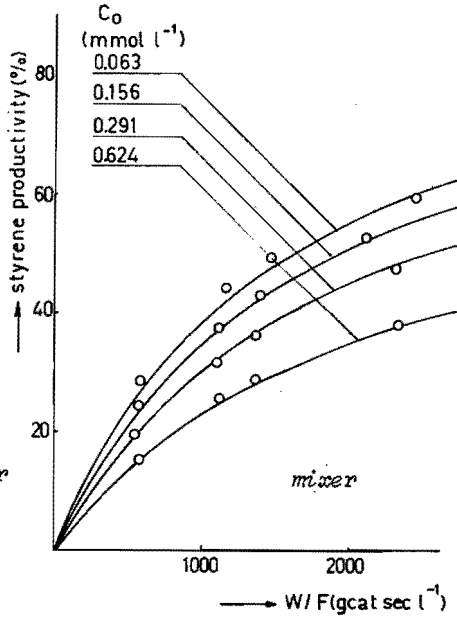

Fig. 5.11

Styrene productivities corrected for non-ideal reactor performance versus W/F: temperature 495°C.
Curves calculated with parameter estimates of table 5.5.

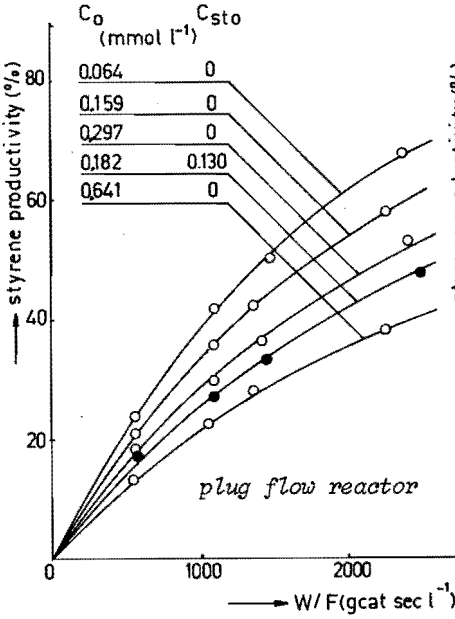

Fig. 5.12

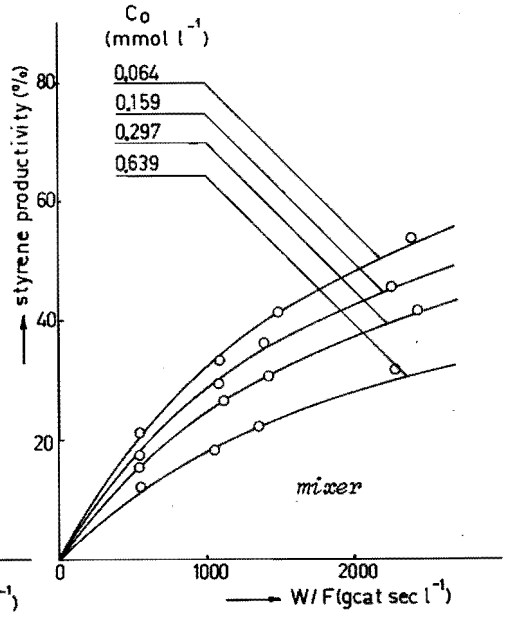

Fig. 5.13

Styrene productivities corrected for non-ideal reactor performance versus W/F: temperature 480°C.
Curves calculated with parameter estimates of table 5.5.

temp.	$\hat{k}$	$\hat{KE}$	$\hat{KS}_{int}$	SS*
°C	l (g cat sec)$^{-1}$	l mmol^{-1}	l mmol^{-1}	
495	7.47×10^{-4}	2.03	2.70	5.6×10^{-3}
480	5.53×10^{-4}	1.82	3.08	3.8×10^{-3}
465	3.98×10^{-4}	1.74	3.14	7.1×10^{-3}

* j = 1 to 36

Table 5.5 Estimates for the kinetic constants k, KE and KS calculated with the corrected styrene productivity data of both plug-flow and stirred reactor experiments.

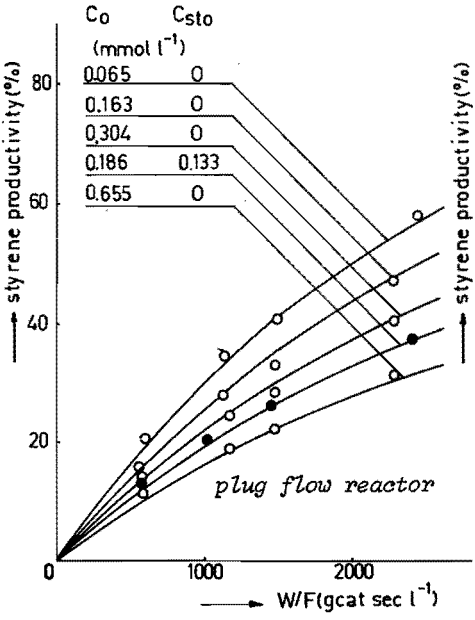

Fig. 5.14

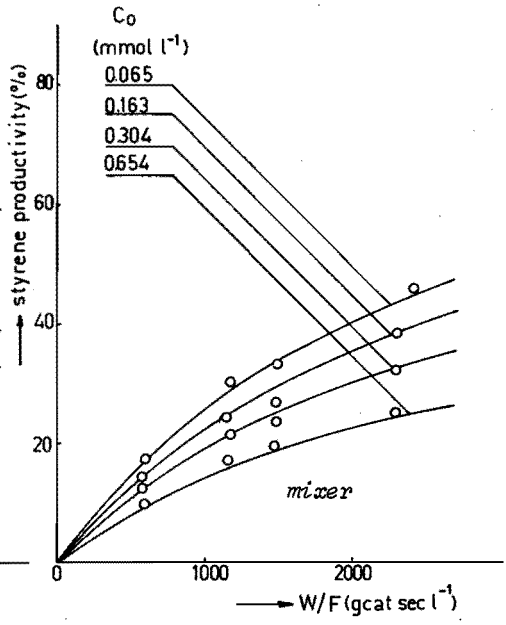

Fig. 5.15

Styrene productivities corrected for non-ideal reactor performance versus W/F: temperature 465°C. Curves calculated with parameter estimates of table 5.5.

5.5. COMPUTATION OF THE ERROR IN THE ESTIMATED PARAMETERS

An Algol 60 procedure described by Linssen (11) can be used to calculate the standard deviations of a set of parameters, estimated with least squares. As the method comprises a linearization step, the generated matrix is only exactly equal to the variance-covariance matrix for linear models. Nevertheless, for non-linear models the method gives a useful approximation.

The calculated approximations of the variance-covariance matrices for the parameters of table 5.5 are given in table 5.6. In it the variances of $\hat{K}S_{dif}$ have been given as well. The values for $\hat{K}S_{dif}$ are lower than for $\hat{K}S_{int}$, but the differences are statistically not significant.

Table 5.6 Variance-covariance matrices of the parameter estimators $\hat{k}$, $\hat{KE}$ and $\hat{KS}_{int}$ calculated from the integral data, and variances of $\hat{KS}_{dif}$.

temp.		$\hat{k}' = \hat{k} \times 10^4$	$\hat{KE}$	$\hat{KS}_{int}$	$\sigma^2(\hat{KS}_{dif})$
	$\hat{k}'$	2.22×10^{-2}	1.35×10^{-2}	2.44×10^{-2}	
495	$\hat{KE}$	1.35×10^{-2}	2.54×10^{-2}	-1.29×10^{-2}	
	$\hat{KS}_{int}$	2.44×10^{-2}	-1.29×10^{-2}	9.61×10^{-2}	3.96×10^{-2}
	$\hat{k}'$	1.43×10^{-2}	1.09×10^{-2}	2.48×10^{-2}	
480	$\hat{KE}$	1.09×10^{-2}	2.66×10^{-2}	-1.57×10^{-2}	
	$\hat{KS}_{int}$	2.48×10^{-2}	-1.57×10^{-2}	0.149	0.85×10^{-2}
	$\hat{k}'$	0.89×10^{-2}	0.95×10^{-2}	2.27×10^{-2}	
465	$\hat{KE}$	0.95×10^{-2}	2.94×10^{-2}	-1.90×10^{-2}	
	$\hat{KS}_{int}$	2.27×10^{-2}	-1.90×10^{-2}	0.223	0.34×10^{-2}

Moreover, we have no physical or chemical reason to suppose that the two values stem from different populations and thus we assume that both $\hat{KS}_{dif}$ and $\hat{KS}_{int}$ are estimators of one KS. These two estimators, which have different variances, were combined. An often applied statistical method for this is to determine the weighted combination:

$$\hat{KS} = \lambda \hat{KS}_{int} + (1-\lambda)\, \hat{KS}_{dif} \qquad (5.16)$$

such that the variance of the joint parameter estimate $\hat{KS}$ is minimum. This condition is met for

$$\lambda = \sigma^2 (\hat{KS}_{dif}) / \{ \sigma^2 (\hat{KS}_{int}) + \sigma^2 (\hat{KS}_{dif}) \}$$

The new variance-covariance matrices for $\hat{k}$, $\hat{KE}$ and the joint estimate $\hat{KS}$ are obtained from the matrices of table 5.6 by multiplying the elements of the row and the column, corresponding to $\hat{KS}$, by appropriate values of λ. These new matrices, together with the values of the parameters and the standard deviations of these estimators are given in table 5.7. The theoretical curves, calculated with the parameter estimates of table 5.7, did not deviate visibly from the curves shown in figures 5.10 to 5.15.

Some general principles of the error estimation procedure have been given in appendix IV.

5.6. THE CONFIDENCE REGIONS OF THE KINETIC PARAMETERS

In the preceding section the standard deviations of $\hat{k}$, $\hat{KE}$ and $\hat{KS}$ have been considered separately. However, the joint confidence intervals of a set of parameters are to be preferred to the perpendicular confidence intervals, (standard deviations) since only the former give information about the sets of $\hat{k}$, $\hat{KE}$ and $\hat{KS}$ values that are consistent with the experimental results.

The joint confidence regions, which contain k, KE and KS within a certain confidence, have elliptical contours. An almost identical method of calculating confidence regions of model parameters has been reported by German (12) and Behnken (13). A brief explanation of the procedure has been given in appendix IV.

If the parameters are estimated by a non-linear least squares method, for reasons mentioned in section 5.5 and

Table 5.7 The parameter estimators $\hat{k}$, $\hat{KE}$ and $\hat{KS}$ and their variance-covariance matrices.

temp.	$\hat{k}$	s.d.	$\hat{KE}$	s.d.	$\hat{KS}$	s.d.*
°C	l (g cat sec)$^{-1}$		l mmol^{-1}		l mmol^{-1}	
495	7.47×10^{-4}	0.15×10^{-4}	2.03	0.16	2.28	0.17
480	5.53×10^{-4}	0.12×10^{-4}	1.82	0.16	2.44	0.11
465	3.98×10^{-4}	0.09×10^{-4}	1.74	0.17	2.71	0.06

temp.		$\hat{k}' = \hat{k}\times10^{4}$	$\hat{KE}$	$\hat{KS}$
	$\hat{k}'$	2.22×10^{-2}	1.35×10^{-2}	0.711×10^{-2}
495	$\hat{KE}$	1.35×10^{-2}	2.54×10^{-2}	-0.376×10^{-2}
	$\hat{KS}$	0.711×10^{-2}	-0.376×10^{-2}	2.80×10^{-2}
	$\hat{k}'$	1.43×10^{-2}	1.09×10^{-2}	0.134×10^{-2}
480	$\hat{KE}$	1.09×10^{-2}	2.66×10^{-2}	-0.085×10^{-2}
	$\hat{KS}$	0.134×10^{-2}	-0.085×10^{-2}	1.26×10^{-2}
	$\hat{k}'$	0.892×10^{-2}	0.095×10^{-2}	0.034×10^{-2}
465	$\hat{KE}$	0.095×10^{-2}	2.94×10^{-2}	-0.028×10^{-2}
	$\hat{KS}$	0.034×10^{-2}	-0.028×10^{-2}	0.335×10^{-2}

* s.d. = standard deviation

in appendix IV, only approximations of the confidence regions can be determined. The regions, calculated with the variance-covariance matrices of table 5.7, are given in figure 5.16. The ellipses given in this figure are the projections of the confidence contours on the k-KE and

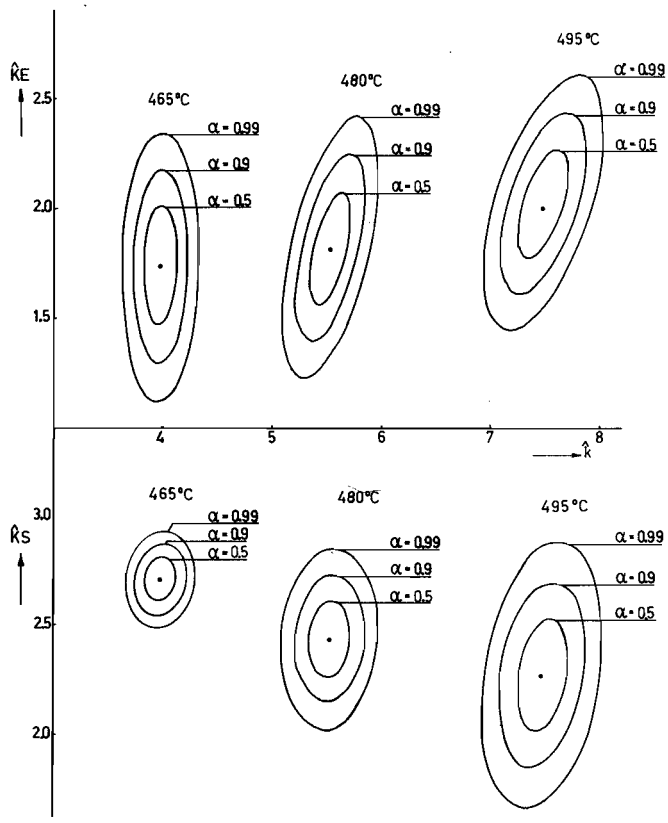

Fig. 5.16 Projections of the confidence regions of the parameter estimators on the k - KE and the k - KS plane; α = probability level.

the k-KS planes respectively. In figure 5.17 a three-dimensional representation of the 90% confidence region at 480°C is given.

The probability level α, for example α = 99%, means that, if a sufficiently large number of experiments is carried out, in one out of a hundred cases the actual set of parameters is situated outside the determined confidence region.

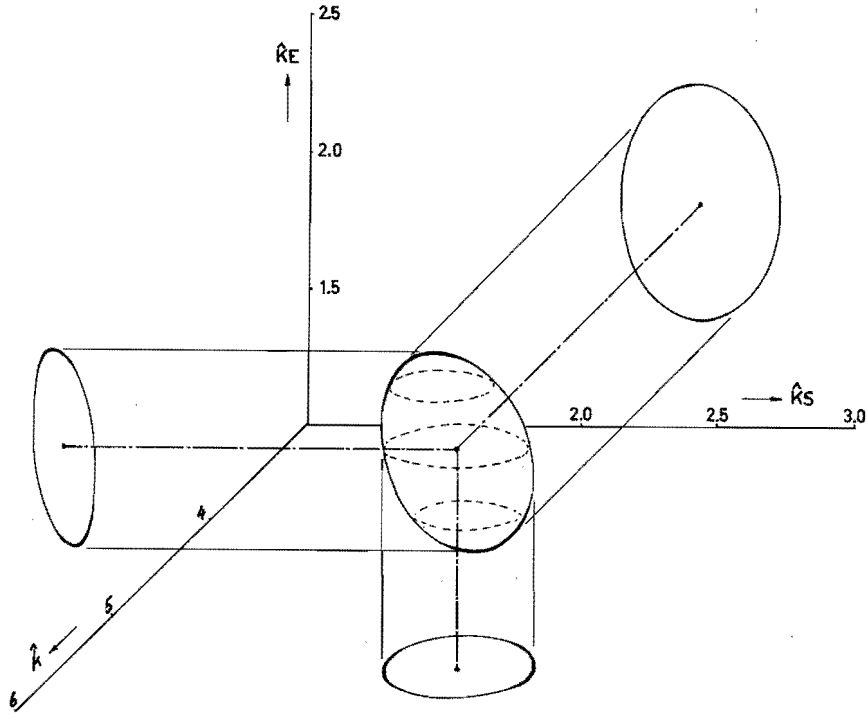

Fig. 5.17 Three dimensional representation of the 90%-confidence region of the parameter estimators at 480°C.

5.7. FINAL REMARKS

Discrimination on statistical grounds between the dual site model (equation 5.1) and the single site model (equation 5.3) was not possible with the results of the integral experiments only. This means that for both models sets of parameter estimates can be calculated so that the residual sums of squares of the differences between the observed and the calculated concentrations do not differ significantly. The results of the differential experiments shown in figures 5.3 and 5.4, however, clearly demonstrate that the single site model is to be preferred.

It should be noted that in equation 5.4 we have assumed that the ethylbenzene concentration is equal to $c_o - c_{St}$. However, for our experiments the selectivity for styrene was 97%, with a standard deviation of 1%. Therefore, the actual concentration of ethylbenzene should be $c_o - 1.03\ c_{St}$. When taking this into account, the values for $\hat{k}$ given in table 5.7 should be increased by about 2%. From the estimators $\hat{k}$ of table 5.7 an energy of activation of 23 kcal mol^{-1} was calculated. Because of the high relative errors of $\hat{K}E$ and $\hat{K}S$, no heats of adsorption for ethylbenzene and styrene were calculated.

Kinetic expressions and their appropriate parameters were not evaluated for the formation of benzene and toluene because the concentrations of these by-products were very low and consequently were determined with rather low accuracy.

The error in the values for c_H, calculated with equation 5.5, has no noticeable effect on the calculated parameter estimates and therefore it was neglected in the calculation of the error of those parameters.

It can be shown that the corrected experimental results in the CSGSR can be predicted with parameter estimates calculated from the corrected plug flow reactor data or vice versa. On statistical grounds the kinetic constants

of table 5.5 were calculated with the combined information from plug flow reactor and CSGSR.

LITERATURE CHAPTER 5

1. Satterfield, C.N., and Sherwood, T.H., "The role of diffusion in catalysis", Addison-Wesley Publishing Company, Reading (Mass.) 1963.
2. Boundy, R.H., and Boyer, R.F., "Styrene Its Polymers, Copolymers and Derivatives". Reinhold Publishing Corp., New York, 1952.
3. Heynen, H.W.G., and van der Baan, H.S., J. Catal. in press.
4. Lootsma, F.A., Thesis, Eindhoven, 1970.
5. Broyden, C.G., J. I.M.A. 6, 222 (1970).
6. Fletcher, R., The Comp. J. 13, 317 (1970).
7. Shanno, D.F., Math. of Comp. 24, 647 (1970).
8. Ebach, E.A., and White, R.R., AIChE J. 4, 161 (1958).
9. Mc. Henry, K.W., and Wilhelm, R.H., AIChE J. 3, 83 (1957).
10. Pasquon, I., and Dente, M., J. Catal. 1, 508 (1962).
11. Linssen, H.N., Internal Report Eindhoven University of Technology, Department of Mathematics, 1973.
12. German, A.L., Thesis, Eindhoven, 1970.
13. Behnken, D.W., J. Polym. Sci. A 2, 645 (1964).

CHAPTER 6

DEHYDROGENATION MECHANISM OF ALKYLBENZENES OVER URANIUM-DIOXIDE

6.1. INTRODUCTION

The hydrogenation and dehydrogenation of non-aromatic hydrocarbons over various metal oxides has been studied extensively (1,2), but practically no information about the dehydrogenation mechanism of alkylbenzenes has been given in the literature. In this chapter a few orienting experiments are described which allow some tentative conclusions.

The thermal decomposition of alkylbenzenes has been studied by, among others, Badger (3) and Leigh (4). Besides cracking products like benzene and toluene, dehydrogenation products like styrene from ethylbenzene and methylstyrenes from propylbenzenes were also found. Badger explains the presence of these dehydrogenation products as follows. Initial decomposition of n-alkylaromatics, with at least two alkylcarbon atoms, occurs by rupture of a C-C bond to give benzyl radicals, e.g.

$$C_6H_5-CH_2-CH_3 \longrightarrow C_6H_5-\dot{C}H_2 + \dot{C}H_3$$

The resulting primary radicals undergo further reactions leading to other radicals and molecules. Hydrogen abstraction from alkylbenzenes by any radical is expected to occur chiefly at the α-carbon atom. The secondary radical thus formed decomposes to give the dehydrogenation product, e.g.

$$C_6H_5-CH_2-CH_3 + \dot{C}H_3 \longrightarrow CH_4 + C_6H_5-\dot{C}H-CH_3$$

$$C_6H_5-\dot{C}H-CH_3 \longrightarrow C_6H_5-CH=CH_2 + \dot{H}$$

On non-acidic metal oxide catalysts alkylbenzenes are preponderently dehydrogenated. This has been described by Pines (5,6) for butylbenzenes and by Tung (7) and Richardson (8) for cumene. In both cases the authors have opted for a free radical dehydrogenation mechanism. In their view the catalyst plays only a role in the formation of the initial radical:

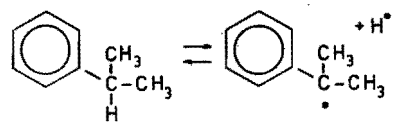

In contrast to the thermal free radical mechanism, where initially a C-C bond breaks, in the catalytic reaction the first step is rupture of a C-H bond.

Cracking of alkylbenzenes over catalysts containing acid sites (e.g. catcracking catalysts), gives predominantly benzene and the corresponding alkene (9). This reaction occurs via a carbonium ion mechanism. Tung (7), by testing a number of catalysts, has shown that the product distribution of the cumene cracking can be used as a measure of the ratio of carbonium ion and free radical type activity of catalysts.

Both Tung and Pines suggest that for the dehydrogenation of alkylaromatics the catalyst only plays a role in the initial step and that the subsequent reaction occurs via free radicals. Burwell (1) and Kokes (2), however, found evidence that, at least during the hydrogenation of alkenes, the catalyst plays an important role in the sequential reaction steps. Kokes studied the hydrogenation of ethylene over ZnO at room temperature. IR spectroscopy measurements proved the existence of Zn-H and O-H surface species when hydrogen is adsorbed on ZnO. After addition of ethylene to the system, a Zn-ethyl bond appeared in the

IR spectrum, while the intensity of the Zn-H bond decreased. Ethylene adsorbed on the ZnO surface is believed to be a surface π-complex. On the principle of micro-reversibility one would therefore expect that the dehydrogenation reaction would also proceed via hydrocarbon species adsorbed on the catalytic surface.

6.2. EXPERIMENTAL AND RESULTS

Ethylbenzene, n-propylbenzene and cumene were dehydrogenated over pure uraniumdioxide (Catalyst A) in the plug flow reactor (figure 2.2) in a way similar to the one described in section 5.2. The results and the reaction conditions of these experiments are given in the tables 6.1, 6.2 and 6.3. As shown in table 6.1, ethylbenzene gives styrene with a selectivity of about 97%; the by-products are benzene and toluene. In the gaseous product after the cold trap, we found, besides hydrogen, methane and ethylene which are formed together with toluene and benzene respectively. For the experiments with cumene, reported in table 6.2, the temperature was reduced from 520°C to 480°C. At 520°C the catalyst deactivated rather quickly, presumably as a result of coke deposition. At the lower temperature the reaction rates were of the same order as those found for ethylbenzene at 520°C. Cumene gives α-methylstyrene with a selectivity of about 96% and benzene, toluene and styrene as by-products. In the condensed reation product only very small amounts of β-methylstyrene were detected (α-MS/β-MS ≈ 100). Table 6.3 gives the results of the n-propylbenzene dehydrogenation. The two major products are α and β-methylstyrene. The selectivity for methylstyrenes varied between 90 and 93%. Beside styrene, small amounts of benzene and toluene, but no detectable amounts of cumene were found. In the gaseous reaction

Table 6.1 Dehydrogenation of ethylbenzene over 1 g pure uraniumdioxide (catalyst A) at 520°C.

c_o	W/F	productivities			selectivity
		P_B	P_T	P_{St}	(for St)
mmol l^{-1}	g cat sec l^{-1}	mol %			%
0.057	149	0.2	0.2	15.3	97.4
0.057	196	0.2	0.2	18.4	97.7
0.057	284	0.3	0.3	23.3	97.7
0.057	566	0.6	0.6	38.4	97.4
0.079	152	0.2	0.2	14.4	97.2
0.079	196	0.2	0.2	17.2	97.4
0.079	287	0.3	0.3	23.5	97.6
0.079	563	0.5	0.4	37.9	97.7
0.123	152	0.1	0.2	11.6	97.0
0.123	196	0.1	0.2	14.1	97.9
0.123	287	0.2	0.2	17.6	97.8
0.123	563	0.4	0.4	30.6	97.5
0.203	152	0.1	0.2	9.4	96.9
0.203	196	0.1	0.2	11.4	97.4
0.203	287	0.1	0.2	15.7	98.3
0.203	567	0.2	0.3	23.9	98.3

Table 6.2 Dehydrogenation of cumene over 1 g pure uraniumdioxide (catalyst A) at 480°C.

c_o	W/F	productivities				selectivity
		P_B	P_T	P_{St}	$P_{\alpha\text{-MS}}$	(for α-MS)
mmol l^{-1}	g cat sec l^{-1}	mol %				%
0.021	149	0.5	0.5	0.8	31.0	94.4
0.021	200	0.6	0.5	0.6	40.3	95.9
0.021	294	0.8	0.6	0.7	48.2	95.7
0.021	582	1.3	0.9	0.8	66.3	95.7
0.034	152	0.3	0.3	0.4	25.2	96.5
0.034	200	0.4	0.3	0.6	33.2	96.4
0.034	294	0.5	0.4	0.6	37.7	97.0
0.034	574	0.7	0.4	0.5	55.7	97.3
0.056	152	0.2	0.3	0.7	18.0	93.2
0.056	200	0.3	0.2	0.5	22.6	95.7
0.056	294	0.3	0.3	0.6	29.6	95.9
0.056	582	0.5	0.4	0.5	44.4	97.0
0.071	152	0.2	0.2	0.6	15.7	93.9
0.071	203	0.2	0.2	0.6	19.1	94.9
0.071	294	0.3	0.3	0.5	25.6	95.8
0.071	582	0.5	0.4	0.5	39.9	96.8

Table 6.3 Dehydrogenation of n-propylbenzene over 5 g pure uraniumdioxide (catalyst A).

temp.	c_o	W/F	productivities					sel.*	$\frac{P_{\beta\text{-MS}}}{P_{\alpha\text{-MS}}}$
			P_B	P_T	P_{St}	$P_{\alpha\text{-MS}}$	$P_{\beta\text{-MS}}$		
°C	mmol l^{-1}	g cat sec l^{-1}	mol %					%	
carrier gas: nitrogen									
500	0.207	1137	0.2	0.1	0.2	1.0	4.5	92	4.5
500	0.207	1705	0.2	0.1	0.3	1.2	5.7	92	4.8
500	0.207	3410	0.4	0.2	0.5	2.3	10.7	92	4.6
500	0.207	6820	0.7	0.5	0.8	3.9	17.6	91	4.5
520	0.202	1108	0.2	0.1	0.3	1.2	5.7	92	4.6
520	0.202	1662	0.3	0.2	0.3	1.8	8.1	93	4.5
520	0.202	3325	0.6	0.3	0.6	3.3	14.1	91	4.3
520	0.202	6650	0.9	0.6	1.1	5.6	24.1	92	4.3
carrier gas: nitrogen + 1 mol % hydrogen									
500	0.207	1137	0.2	0.1	0.2	0.85	3.8	90	4.7
500	0.207	1705	0.2	0.1	0.3	1.05	4.7	91	4.5
500	0.207	3410	0.3	0.2	0.5	2.1	9.2	92	4.4
500	0.207	6820	0.7	0.5	0.7	3.8	16.0	91	4.3
520	0.202	1108	0.2	0.1	0.2	1.0	4.5	92	4.5
520	0.202	1662	0.3	0.2	0.3	1.4	6.7	91	4.8
520	0.202	3325	0.5	0.3	0.6	2.6	11.6	91	4.5
520	0.202	6650	0.8	0.6	1.1	4.7	19.8	91	4.2

*) Selectivity for α-methylstyrene plus β-methylstyrene.

products of the propylbenzenes, methane, ethylene and propylene were found.

6.3. DISCUSSION

Starting from cumene, α-methylstyrene and hydrogen are formed almost exclusively. When these data are compared to those presented by Tung (7) on cumene, it is found that our product distribution is similar to the distribution that is ascribed by Tung to a radical type of reaction. Our data on ethylbenzene and n-propylbenzene also show high selectivities for dehydrogenation, which is in accordance with such a reaction mechanism.

For uranium oxide on alumina (see tables III.1, III.2 and III.3 of appendix III) the product distribution also indicates a radical type of mechanism, as hardly any products requiring a carbonium ion mechanism are found. Consequently, we conclude that catalyst A and catalyst B contain no, or hardly any, acidic sites.

It seems reasonable to assume that on uraniumdioxide, just as on chromia, alumina and zincoxide, the first reaction step is cleavage of a C-H bond. We suppose that, similarly to the hydrogen abstraction by free radicals, in the catalytic process the first hydrogen atom is split from the α-carbon atom. According to the mechanism for ethylene hydrogenation over chromia and zincoxide, as proposed by Burwell and Kokes, we suggest the following dehydrogenation mechanism for ethylbenzene:

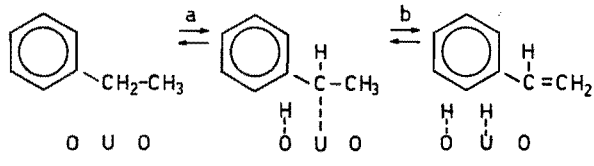

The dehydrogenations of cumene and n-propylbenzene are believed to occur similarly. Both α and β-methylstyrene are found in the product mixture from propylbenzene, whereas cumene gives α-methylstyrene and only a very small amount of β-methylstyrene (α-MS/β-MS ≃ 100). We suggest the following reaction route:

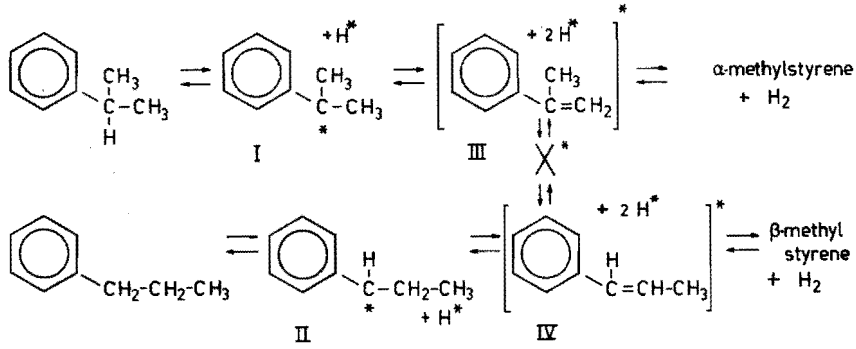

An atom or molecule bound to the surface is here designated by * .

It seems reasonable to postulate that the isomerization intermediate X is a phenyl cyclopropane type of surface species. Isomerization reactions of alkanes and butylbenzenes over non-acidic metal oxide catalysts have been frequently proposed to occur via cyclo-C3 intermediates (10, 11, 12).

The almost complete absence of β-methylstyrene in the dehydrogenation product mixture of cumene may indicate that the isomerization species X is hardly formed during cumene dehydrogenation. One reason could be that the formation of X, starting from species III, is energetically unfavourably compared to the desorption of that species. Another explanation might be that the frequency factor for the reaction starting from species III is much smaller than that starting from IV.

The ratio of the productivities of α and β-methylstyrene in the propylbenzene dehydrogenation product mixture is practically independent of the reaction conditions, particularly the reaction temperature. For the proposed reaction route this implies that, starting from surface species IV, the energy of activation for the desorption of IV and for the formation of the isomerization intermediate X are almost equal.

Cumene is not found in the dehydrogenation product mixture of propylbenzene, in spite of the fact that both α-methylstyrene and hydrogen are present, because under the prevailing conditions the equilibrium concentration of cumene was not detectable.

In the foregoing we have avoided the question of adsorption of the benzene ring. An indication of the assumption that the benzene ring is not adsorbed on the catalyst surface is provided by the change in the product composition during the reduction of the catalyst, as shown in figure 3.2. Initially, ethylbenzene is completely oxidized, i.e. oxygen from the lattice reacts with atoms of the benzene ring, which therefore must be in contact with the catalyst. When the reduction of the catalyst proceeds, the benzene ring oxidation stops (although the catalyst still yields oxygen for other oxidation reactions), indicating that no reactive sites for benzene ring adsorption are available anymore.

Although no definite conclusions can be drawn from the experiments described in this chapter, there is no contradiction between these observations and the kinetic model.

LITERATURE CHAPTER 6

1. Burwell, R.L., Jr., Haller, G.J., Taylor, K.C., and Read, J.F., Advan. Catal. 20, 1 (1969).
2. Kokes, R.J., and Dent, A.L., Advan. Catal. 22, 1 (1972).
3. Badger, G.M., and Spotswood, T.M., J. Chem. Soc. 276, 4420 (1960).
4. Leigh, C.H., and Szwarc, M.J., J. Chem. Phys. 20, 844 (1952).
5. Pines, H., and Goetschel, C.T., J. Catal. 6, 371 (1966).
6. Pines, H., and Goetschel, C.T., J. Catal. 6, 380 (1966).
7. Tung, S.E., and Mc Ininck, E., J. Catal. 4, 586 (1965).
8. Richardson, J.T., J. Catal. 9, 182 (1967).
9. Prater, C.D., and Lago, R.M., Advan. Catal. 8, 293 (1956).
10. Anderson, J.R., Advan. Catal. 23, 1, (1973).
11. Pines, H., and Goetschel, C.T., J. Org. Chem. 30, 3530 (1965).
12. Pines, H., and Csicsery, S.M., J. Catal. 1, 313 (1962).

APPENDIX I

CALCULATION OF PRODUCTIVITY AND SELECTIVITY

The calculation procedure for a fixed bed experiment, with both ethylbenzene and styrene in the feed gas is given below. The parts of the apparatus which are significant are shown in figure I.1.

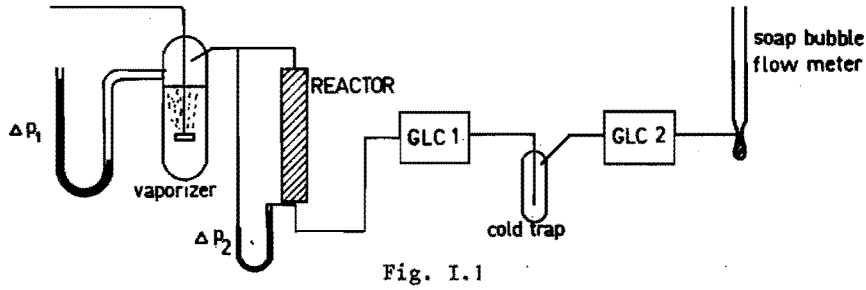

Fig. I.1

Benzene (B), toluene (T) and styrene (St) are formed from ethylbenzene (EB) according to the following reactions:

$$EB \rightarrow St + H_2 \qquad (I.1)$$

$$EB \rightarrow B + C_2H_4 \qquad (I.2)$$

$$EB + H_2 \rightarrow T + CH_4 \qquad (I.3)$$

Moreover, during experiments with carbondioxide as carrier gas the water gas shift reaction takes place:

$$CO_2 + H_2 \rightarrow CO + H_2O \qquad (I.4)$$

During an experiment the following data are determined:
a) reactor temperature T_R (^oC)
b) vapour pressures p_{EB} and p_{St} (mm Hg)

c) room temperature T_1 (^oC)
d) barometric pressure p_{bar} (mm Hg)
e) reactor inlet pressure = pressure above liquid in the vaporizer $p_i = p_{bar} + \Delta p_1$ (mm Hg)
f) pressure drop over the catalyst Δp_2 (mm Hg)
g) gas flow rate after cold trap (pressure p_{bar}, temperature T_1) ϕ_1 (l h^{-1})
h) from GLC_2 : $\%H_2$ in gas flow after cold trap
i) from GLC_1 : hydrocarbon surface areas A_B, A_T, A_{EB}, A_{St}.

For the various compounds the following symbols are used:

$co2_o$	= mmol h^{-1} CO_2	entering the reactor
eb_o	= mmol h^{-1} EB	"
st_o	= mmol h^{-1} St	"
co2	= mmol h^{-1} CO_2	leaving the reactor
eb	= mmol h^{-1} EB	"
st	= mmol h^{-1} St	"
b	= mmol h^{-1} B	"
t	= mmol h^{-1} T	"
met	= mmol h^{-1} CH_4	"
et	= mmol h^{-1} C_2H_4	"
h2	= mmol h^{-1} H_2	"
h2o	= mmol h^{-1} H_2O	"
co	= mmol h^{-1} CO	"

tot mol = total mole flow after the cold trap (mmol h^{-1})

For the hydrocarbons entering the reactor applies:

$$eb_o = \frac{p_{EB}}{p_i - p_{EB} - p_{St}} \times co2_o \qquad \text{mmol } h^{-1} \qquad \text{(I.5)}$$

and

$$st_o = \frac{p_{St}}{p_i - p_{EB} - p_{St}} \times co2_o \qquad \text{mmol } h^{-1} \qquad \text{(I.6)}$$

From the hydrocarbon analysis on GLC_1 (see §2.3) follows:

$$b = eb_o \, \gamma_B \, A_B \, / \, A_{EB_o} \qquad \text{mmol } h^{-1} \qquad \text{(I.7)}$$

$$t = eb_o \, \gamma_T \, A_T \, / \, A_{EB_o} \qquad \text{mmol } h^{-1} \qquad \text{(I.8)}$$

$$eb = eb_o \, 1.00 \, A_{EB} \, / \, A_{EB_o} \qquad \text{mmol } h^{-1} \qquad \text{(I.9)}$$

$$st = eb_o \, \gamma_{St} \, A_{St} \, / \, A_{EB_o} \qquad \text{mmol } h^{-1} \qquad \text{(I.10)}$$

$$+$$

$$b + t + eb + st = eb_o \, (\gamma_B A_B + \gamma_T A_T + A_{EB} + \gamma_{St} A_{St}) / A_{EB_o}$$

or:

$$eb_o + st_o = eb_o \sum_i \gamma_i A_i \, / \, A_{EB_o} \qquad \text{(I.11)}$$

Division by eb_o:

$$1 + \frac{st_o}{eb_o} = \sum_i \gamma_i A_i \, / \, A_{EB_o}$$

As $\frac{st_o}{eb_o} = \frac{p_{St}}{p_{EB}}$ we can calculate A_{EB_o}:

$$A_{EB_o} = \sum_i \gamma_i A_i \, / \, (1 + \frac{p_{St}}{p_{EB}}) \qquad \text{(I.12)}$$

A_{EB_o} is the fictitious surface area that ethylbenzene should have under conditions identical with the actual

ones, but without any conversion. With equations I.7 - I.12 the number of moles of the various hydrocarbons can be calculated after $co2_o$ is known.

In the cold trap the aromatics and water are condensed and therefore:

$$\text{tot mol} = co2 + met + et + h2 + co$$
$$= co2_o + h2 + met + et \qquad \text{mmol } h^{-1} \quad (I.13)$$

With I.2 and I.3 we find:

$$\text{tot mol} - h2 = co2_o + b + t \qquad \text{mmol } h^{-1} \quad (I.14)$$

tot mol is calculated from ϕ_1:

$$\text{tot mol} = \frac{\phi_1 \left| \frac{273}{273+T_1} \right| \frac{p_{bar}}{760}}{22.4} \times 1000 \qquad \text{mmol } h^{-1} \quad (I.15)$$

and h2 we found with:

$$h2 = \%H_2 \times \text{tot mol} / 100 \qquad (I.16)$$

Combination of the equations I.14, I.7 and I.8 results in:

$$\text{tot mol} - h2 = co2_o + eb_o \left| \frac{\gamma_B A_B + \gamma_T A_T}{A_{EB_o}} \right| \qquad (I.17)$$

With I.5:

$$\text{tot mol} - h2 = co2_o \left| 1 + \frac{p_{EB}}{p_i - p_{EB} - p_{St}} \left(\frac{\gamma_B A_B + \gamma_T A_T}{A_{EB_o}} \right) \right|$$

or:

$$co2_o = (\text{tot mol} - h2)\left|1+\frac{p_{EB}}{p_i - p_{EB} - p_{St}}\left(\frac{\gamma_B A_B + \gamma_T A_T}{A_{EB_o}}\right)\right|^{-1}$$

$$\text{mmol } h^{-1} \quad \text{(I.18)}$$

Now (a) eb_o, st_o, eb, st, b, and t, (b) the productivities P_i and the conversion and the selectivity are calculated:

$$P_B = b/eb_o, \qquad P_T = t/eb_o, \qquad P_{St} = (st - st_o)/eb_o,$$

$$\text{conversion} = P_B + P_T + P_{St}$$

$$\text{selectivity} = P_{St}/\text{conversion}$$

The pressure and the total number of moles varies over the catalyst bed. This variation should be taken into account when calculating the contact time W/F (g cat sec l^{-1}), and the concentrations in the reactor.
For fixed bed experiments the pressure drop over the bed is at most 1 mm Hg; moreover, no ethylbenzene vapour pressures above 30 mm Hg were applied. We decided to calculate the average feed rate F at $p = p_i - \frac{1}{2}\Delta p_2$ and at conversion half the total conversion. The total number of moles then equals to:

$$co2_o + eb_o + st_o + \tfrac{1}{2}(st - st_o) + \tfrac{1}{2}b$$

and

$$F = 22.4\text{x}10^{-3}\ (co2_o + eb_o + st_o + \tfrac{1}{2}(st - st_o) + \tfrac{1}{2}b)\frac{273+T_R}{273}\frac{760}{p_{bar}}\ 1h^{-1}$$

With the average F-values the reaction product and feed concentrations were also calculated:

$$c_{EB_o} = eb_o/F, \qquad c_{St_o} = st_o/F \qquad \text{mmol } l^{-1}$$

$$c_{EB} = eb/F, \quad c_B = b/F, \quad c_T = t/F, \quad c_{St} = st/F \text{ mmol } l^{-1}$$

The error, introduced in the kinetic parameters by assuming the reaction volume to be constant, can be shown to be negligible.

Calculations of mixer experiments were analogous, except that in this case the average reaction volume was calculated at reactor outlet conversion.

APPENDIX II

DATA USED FOR VARIOUS CALCULATIONS

Reactor A:

catalyst bed cross section	44.5×10^{-4}	m^2
height catalyst bed	4.4×10^{-2}	m

Reactor B:

catalyst bed cross section	3.1×10^{-4}	m^2
height catalyst bed	2.7×10^{-2}	m

Silicon carbide:

average particle diameter, d_p	1.2×10^{-3}	m
external void fraction, ε	0.5	

Catalyst B:

average particle diameter, d_p	7.2×10^{-4}	m
external void fraction, ε	0.35	
internal pore void fraction, θ	0.52	
bulk density, ρ_b	1000	kg m^{-3}
particle density, ρ_p	1540	kg m^{-3}
average pore radius, r_p	46×10^{-10}	m

		Ref.
Viscosity:		
carbondioxide (495°C), μ_{CO_2}	3.3×10^{-5} N sec m^{-2}	(1)
nitrogen (500°C), μ_{N_2}	3.5×10^{-5} N sec m^{-2}	(1)
Density:		
carbondioxide (495°C), ρ_{CO_2}	0.70 kg m^{-3}	(1)
nitrogen (500°C), ρ_{N_2}	0.45 kg m^{-3}	(1)
Specific heat:		
carbondioxide (495°C), c_p	0.28 kcal $(kg\,°C)^{-1}$	(1)
Diffusion coefficient:		
ethylbenzene in CO_2 (495°C), D_{EB}	0.31×10^{-4} m^2 sec^{-1}	(1)

Reference 1 Perry, J.H. "Chemical Engineer's Handbook", Mc Graw-Hill Book Company, New York, 1963.

APPENDIX III

EXPERIMENTAL DATA

Table III.1 Results of kinetic experiments in reactor B at 495°C

j	c_o	c_{St_o}	W/F	D/uL	n	productivities				selectivity	P_{St} in ideal reactor
						P_B	P_T	P_{St}	P_{H_2}		
	mmol l^{-1}		g cat sec l^{-1}			mol %				%	mol %
						plug flow reactor					
1	0.628	0	578	0.009	-	0.2	0.4	18.3	8.1	96.8	18.3
2	0.628	0	1084	0.017	-	0.3	0.5	30.0	13.1	97.4	30.2
3	0.628	0	1373	0.022	-	0.3	0.6	34.6	15.5	97.5	34.9
4	0.628	0	2263	0.036	-	0.4	0.7	46.2	18.8	97.7	47.2
5	0.291	0	578	0.009	-	0.2	0.5	22.2	8.1	96.7	22.3
6	0.291	0	1100	0.017	-	0.3	0.6	36.2	13.4	97.6	36.5
7	0.291	0	1374	0.022	-	0.3	0.6	41.8	15.4	97.9	42.3
8	0.291	0	2331	0.037	-	0.6	0.8	57.7	18.7	97.6	59.1
9	0.178	0.127	583	0.009	-	0.3	0.6	24.0		96.4	24.1
10	0.178	0.127	1110	0.017	-	0.5	0.7	37.3		96.9	37.6
11	0.178	0.127	1483	0.024	-	0.6	0.8	44.8		97.0	45.4
12	0.178	0.127	2335	0.037	-	1.0	0.2	55.1		96.2	56.5
13	0.156	0	570	0.009	-	0.2	0.8	27.7		96.5	27.8
14	0.156	0	1120	0.018	-	0.5	0.8	43.5		97.1	43.9
15	0.156	0	1396	0.022	-	0.5	0.9	51.9		97.4	52.5
16	0.156	0	2124	0.034	-	0.9	1.1	64.8		97.0	66.2
17	0.062	0	586	0.009	-	0.3	0.7	33.1		97.1	33.2
18	0.062	0	1155	0.018	-	0.6	1.0	52.2		97.0	52.7
19	0.062	0	1451	0.023	-	0.6	1.0	60.8		97.4	61.4
20	0.062	0	2355	0.037	-	1.2	1.1	75.4		97.2	77.2
							mixer				
21	0.624	0	582	-	5	0.2	0.6	15.7	7.4	95.2	15.5
22	0.624	0	1102	-	9	0.3	0.6	26.2	11.8	96.7	25.8
23	0.624	0	1375	-	11	0.3	0.7	29.5	12.8	96.7	29.0
24	0.624	0	2329	-	17	0.4	1.0	38.8	15.5	96.5	38.2
25	0.291	0	582	-	5	0.3	0.6	19.5	7.2	95.6	19.1
26	0.291	0	1102	-	9	0.3	0.8	31.9	11.0	96.7	31.3
27	0.291	0	1375	-	11	0.3	0.8	36.9	12.7	97.1	36.2
28	0.291	0	2329	-	17	0.6	0.9	48.2	15.5	97.0	47.4
29	0.156	0	575	-	5	0.2	0.8	25.3		96.2	24.8
30	0.156	0	1124	-	9	0.4	0.8	38.9		97.0	38.1
31	0.156	0	1400	-	11	0.6	0.9	44.4		96.7	43.6
32	0.156	0	2127	-	16	1.2	1.0	53.3		96.0	52.4
33	0.063	0	590		5	0.3	0.8	29.0		96.3	28.4
34	0.063	0	1160		9	0.6	0.8	45.3		97.0	44.4
35	0.063	0	1456		11	0.6	0.9	50.3		97.1	49.4
36	0.063	0	2362		17	1.2	1.1	60.0		96.3	58.9

Table III.2 Results of kinetic experiments in reactor B at 480°C

j	c_o	c_{St_o}	W/F	D/uL	n	productivities				selectivity	P_{St} in ideal reactor
						P_B	P_T	P_{St}	P_{H_2}		
	mmol l^{-1}		g cat sec l^{-1}			mol %				%	mol %
						plug flow reactor					
1	0.641	0	550	0.008	-	0.0	0.5	13.4	8.2	96.4	13.4
2	0.641	0	1049	0.016	-	0.2	0.6	22.4	11.7	96.6	22.5
3	0.641	0	1371	0.020	-	0.2	0.6	27.8	13.0	97.2	28.0
4	0.641	0	2253	0.033	-	0.3	0.7	37.2	16.3	97.4	37.9
5	0.297	0	560	0.008	-	0.0	0.5	18.3	6.7	97.3	18.3
6	0.297	0	1107	0.016	-	0.1	0.6	29.1	11.7	97.7	29.3
7	0.297	0	1410	0.021	-	0.2	0.7	35.7	13.4	97.5	36.0
8	0.297	0	2420	0.036	-	0.5	0.9	51.9	17.5	97.4	53.0
9	0.182	0.130	572	0.008	-	0.3	0.8	17.6		94.1	17.6
10	0.182	0.130	1090	0.016	-	0.5	0.9	26.5		95.0	26.7
11	0.182	0.130	1460	0.022	-	0.6	1.0	32.4		95.3	32.7
12	0.182	0.130	2485	0.037	-	0.6	1.0	46.4		96.7	47.5
13	0.159	0	563	0.008	-	0.1	0.6	21.0	8.5	96.8	21.0
14	0.159	0	1080	0.016	-	0.1	0.8	35.3	12.1	97.5	35.5
15	0.159	0	1386	0.021	-	0.3	0.8	42.0	13.5	97.5	42.4
16	0.159	0	2244	0.033	-	0.6	1.0	56.9	15.9	97.3	58.0
17	0.064	0	568	0.008	-	0.3	0.6	23.6		96.3	23.7
18	0.064	0	1078	0.016	-	0.5	0.8	41.5		97.0	41.8
19	0.064	0	1469	0.022	-	0.6	0.8	49.3		97.0	49.8
20	0.064	0	2385	0.035	-	1.1	0.9	66.5		97.1	67.9
							mixer				
21	0.639	0	553	-	5	0.0	0.5	12.3	6.7	96.1	12.1
22	0.639	0	1051	-	9	0.0	0.6	18.5	10.4	96.9	18.2
23	0.639	0	1370	-	11	0.2	0.6	22.4	11.8	96.6	22.0
24	0.639	0	2245	-	16	0.4	1.0	32.5	15.5	95.9	32.0
25	0.297	0	565	-	5	0.0	0.6	15.5	5.9	96.3	15.2
26	0.297	0	1111	-	10	0.3	0.7	26.7	10.3	96.4	26.4
27	0.297	0	1413	-	13	0.3	0.7	30.9	11.4	96.9	30.4
28	0.297	0	2418	-	17	0.6	1.0	42.5	15.9	96.4	41.8
29	0.159	0	568	-	5	0.0	0.8	17.3	6.8	95.6	17.0
30	0.159	0	1084	-	9	0.3	0.9	29.5	10.7	96.1	29.0
31	0.159	0	1389	-	11	0.3	0.9	37.2	11.6	96.9	36.6
32	0.159	0	2246	-	16	0.7	1.0	46.6	14.6	96.5	45.9
33	0.064	0	573	-	5	0.3	0.6	21.2		95.9	20.8
34	0.064	0	1084	-	10	0.5	0.7	33.6		96.6	33.0
35	0.064	0	1474	-	11	0.8	0.8	42.3		96.4	41.6
36	0.064	0	2391	-	16	1.0	1.0	54.9		96.9	54.0

Table III.3 Results of kinetic experiments in reactor B at 465°C

j	c_o	c_{St_o}	W/F	D/uL	n	productivities				selectivity	P_{St} in ideal reactor
						P_B	P_T	P_{St}	P_{H_2}		
	mmol l^{-1}		g cat sec l^{-1}			mol %				%	mol %
						plug flow reactor					
1	0.655	0	592	0.008		0.0	0.4	11.4	5.7	96.6	11.4
2	0.655	0	1150	0.016		0.0	0.5	19.1	9.7	97.4	19.2
3	0.655	0	1447	0.021	-	0.2	0.5	22.4	11.3	97.0	22.6
4	0.655	0	2286	0.033		0.3	0.6	31.3	14.2	97.2	31.8
5	0.304	0	581	0.008		0.0	0.6	14.5	6.3	96.0	14.5
6	0.304	0	1186	0.017		0.2	0.6	24.1	10.1	96.8	24.2
7	0.304	0	1470	0.021	-	0.2	0.7	27.2	11.5	96.8	27.4
8	0.304	0	2293	0.033		0.3	0.7	38.9	15.0	97.5	39.6
9	0.186	0.133	582	0.008		0.2	0.4	13.7		95.8	13.7
10	0.186	0.133	1002	0.014		0.3	0.4	20.6		96.7	20.7
11	0.186	0.133	1461	0.021	-	0.3	0.7	25.6		96.2	25.8
12	0.186	0.133	2405	0.034		0.3	0.8	36.3		97.1	37.0
13	0.163	0	589	0.008		0.0	0.0	15.8	6.3	95.2	15.8
14	0.163	0	1138	0.017		0.1	0.8	27.4	9.5	96.8	27.6
15	0.163	0	1485	0.021	-	0.1	0.9	32.1	11.6	97.0	32.4
16	0.163	0	2301	0.033		0.3	1.0	45.8	14.0	97.2	46.4
17	0.065	0	596	0.009		0.0	0.8	21.0		96.3	21.0
18	0.065	0	1152	0.017		0.3	0.8	34.4		96.9	34.6
19	0.065	0	1486	0.021	-	0.3	0.9	40.2		97.1	40.5
20	0.065	0	2413	0.035		0.4	1.0	57.0		97.6	58.1
							mixer				
21	0.654	0	596		6	0.0	0.4	10.1	5.0	96.2	10.0
22	0.654	0	1153		11	0.0	0.5	17.6	8.8	97.2	17.4
23	0.654	0	1449	-	12	0.2	0.6	19.7	9.9	96.1	19.4
24	0.654	0	2283		19	0.3	0.6	25.7	13.2	96.6	25.4
25	0.304	0	586		5	0.0	0.5	13.0	5.8	96.3	12.8
26	0.304	0	1190		13	0.2	0.6	21.5	9.0	96.4	21.2
27	0.304	0	1473	-	12	0.2	0.7	23.6	9.8	96.3	23.2
28	0.304	0	2295		17	0.3	0.7	32.7	13.0	97.0	32.2
29	0.163	0	594		5	0.0	0.6	14.2	5.7	95.9	14.0
30	0.163	0	1145		11	0.2	0.6	24.5	8.5	96.8	24.1
31	0.163	0	1490	-	12	0.2	0.8	26.9	9.5	96.4	26.4
32	0.163	0	2305		19	0.3	1.0	38.5	12.4	96.7	38.0
33	0.065	0	600		6	0.0	0.5	17.7		97.3	17.4
34	0.065	0	1156		11	0.3	0.6	31.2		97.2	30.8
35	0.065	0	1490	-	12	0.3	0.9	33.6		96.6	33.1
36	0.065	0	2417		20	0.5	1.0	46.6		96.9	45.9

Table III.4 Differential measurements for determination of $\hat{K}S_{dif}$
Reaction conditions: 0.5 g catalyst B;
carrier gas, nitrogen with 1.2 % hydrogen

temp	F	W/F	prod EB	c_{St_o}	$\Delta c_{EB}/(W/F)$	$1/c_{St_o}$	1/r
°C	1 h^{-1}	g cat sec l^{-1}	mol %	mmol l^{-1}	mmol (g cat sec)$^{-1}$	1 $mmol^{-1}$	g cat sec $mmol^{-1}$
495	26.3	68.4	2.71	0.0449	0.178×10^{-4}	22.3	5.62×10^{-4}
-	26.4	68.2	2.63	0.0682	0.263 -	14.7	3.80 -
-	26.5	67.9	2.30	0.1230	0.417 -	8.13	2.40 -
-	26.8	67.2	1.92	0.2781	0.794 -	3.60	1.26 -
-	27.3	66.2	1.34	0.530	1.075 -	1.89	0.93 -
480	25.8	69.8	2.66	0.0457	0.174×10^{-4}	21.9	5.75×10^{-4}
-	25.9	69.5	2.53	0.0695	0.253 -	14.4	3.95 -
-	25.9	69.5	2.23	0.1256	0.403 -	7.96	2.48 -
-	26.3	68.4	1.75	0.2835	0.725 -	3.53	1.38 -
-	26.7	67.4	1.25	0.540	1.000 -	1.85	1.00 -
465	25.3	71.2	2.62	0.0467	0.172×10^{-4}	21.4	5.82×10^{-4}
-	25.4	70.9	2.45	0.0709	0.245 -	14.1	4.08 -
-	25.4	70.9	2.15	0.1230	0.389 -	7.81	2.57 -
-	25.8	69.8	1.61	0.2781	0.667 -	3.46	1.50 -
-	26.1	69.0	1.17	0.530	0.935 -	1.81	1.07 -

APPENDIX IV

STATISTICS

IV.1 LINEAR LEAST SQUARES

Suppose we have a model which can be written in the form:

$$Y = X\beta + \epsilon \qquad \text{(IV.1)}$$

with:

Y = n x 1 vector, the vector of observations
X = n x p matrix, the design matrix
β = p x 1 vector, the parameter vector
ϵ = n x 1 vector, the vector of errors

The errors are normally distributed with $E(\epsilon)=0$ and $Var(\epsilon)=I\sigma^2$.

The sum of squares of the errors is

$$\epsilon'\epsilon = (Y - X\beta)'(Y - X\beta) \qquad \text{(IV.2)}$$

For the vector $\hat{\beta}$, which minimizes $\epsilon'\epsilon$, is found by differentiation of relation IV.2 :

$$X'X\hat{\beta} = X'Y \quad \text{or} \quad \hat{\beta} = (X'X)^{-1}X'Y \qquad \text{(IV.3)}$$

with $Var(\hat{\beta}) = (X'X)^{-1}\sigma^2$.

An estimate of the variance σ^2 is provided by dividing the residual sum of sqares by its degrees of freedom:

$$s^2 = (Y - X\hat{\beta})'(Y - X\hat{\beta}) / (n-p) \qquad \text{(IV.4)}$$

The matrix $(X'X)^{-1} s^2$ is an estimate of the variance-covariance matrix of the parameter estimates $\hat{\beta}$.

In this way, from the differential experiments the variance-covariance matrices of $\hat{\beta}_o$ and $\hat{\beta}_1$ have been determined. Using the principle of propagation of errors, provided that the relative errors of $\hat{\beta}_o$ and $\hat{\beta}_1$ are small, the following expression for the variance of $\hat{KS}_{dif} = \hat{\beta}_o/\hat{\beta}_1$, given in table 5.6, was found:

$$\mathrm{Var}(\hat{KS}_{dif}) \cong \begin{vmatrix} \frac{1}{\hat{\beta}_1} & , & \frac{-\hat{\beta}_o}{\hat{\beta}_1} \end{vmatrix} (X'X)^{-1} s^2 \begin{vmatrix} \frac{1}{\hat{\beta}_1} \\ \frac{-\hat{\beta}_o}{\hat{\beta}_1} \end{vmatrix} \qquad \text{(IV.5)}$$

IV.2 NON-LINEAR LEAST SQUARES

If a model is not linear in the parameters, the least squares estimation procedure loses its great simplicity. As long as the errors can be assumed to be normally distributed, least squares estimators coincide with a class of estimators called maximum likelihood estimators, whose usefulness can be justified from several points of view. Though the assumption of normality is rarely completely met, most of the statistical theory based upon it is not sensitive to slight departures from normality.

Suppose the model is represented by:

$$Y = f(\beta) + \epsilon \qquad \text{(IV.6)}$$

or component i of Y (observation y_i):

$$y_i = f_i(\beta) + e_i$$

In the following we shall use the notation:
β is the vector variable of the general model IV.6, β_o is the value of β in the population, and $\hat{\beta}$ is an estimate of β_o.

This estimate $\hat{\beta}$ of β_o is the value of β for which

$$\sum_{i=1}^{n} \{ y_i - f_i(\beta) \}^2 \qquad \text{(IV.7)}$$

is minimized as a function of β.

It is not possible to determine the variance-covariance matrix in this case. However, an approximation of this matrix can be determined as follows. Expansion of the model function f in a Taylor's series round $\beta = \beta_o$ gives:

$$y_i = f_i(\beta_o) + \sum_{j=1}^{p} \frac{\delta f_i(\beta_o)}{\delta \beta_j} (\beta_j - \beta_{oj}) + \cdots$$

$$i = 1,2,\cdots,n \qquad \text{(IV.8)}$$

Assuming that the terms with partial derivatives of orders not higher than one provide a good approximation of the model function round $\beta = \beta_o$, we find:

$$y_i - c_i = \sum_{j=1}^{p} \frac{\delta f_i(\beta_o)}{\delta \beta_j} \beta_j + e_i \qquad \text{(IV.9)}$$

with: $$c_i = f_i(\beta_o) - \sum_{j=1}^{p} \frac{\delta f_i(\beta_o)}{\delta \beta_j} \beta_{oj}$$

Relation IV.9 is linear in the parameters and thus can be written as:

$$Y - C = X\beta + \epsilon$$

with X an n x p matrix with elements

$$x_{ij} = \frac{\delta f_i(\beta_o)}{\delta \beta_j}$$

Y and C are n x 1 vectors with elements y_i and c_i. Analogously to the linear case we find:

$$\mathrm{Var}(Y-C) = I\,\sigma^2 \quad \text{and}$$

$$\mathrm{Var}(\hat{\beta}) = (\mathcal{X}'\mathcal{X})^{-1}\,\sigma^2 \qquad \text{(IV.10)}$$

IV.3 CONFIDENCE REGIONS

Let the parameter estimator vector be $\hat{\beta}$, having a variance-covariance matrix $\mathcal{X}$ with elements x_{ij}. The boundary of the region with confidence coefficient α in the space of the parameters is formed by the values of $\Delta\hat{\beta} = \beta - \hat{\beta}$ that satisfy the equation:

$$(\Delta\hat{\beta})'\,\mathcal{X}^{-1}(\Delta\hat{\beta}) = p\,F\alpha\,(p,\nu) \qquad \text{(IV.11)}$$

In this equation $F\alpha\,(p,\nu)$ is the α percentage point of the F-distribution with p and ν degrees of freedom. p is the number of parameters and ν is number of degrees of freedom of the variance-covariance matrix.

Working out relation IV.11 for our special case (p=3, ν=33) yields for the formula of the confidence ellipsoid:

$$d_{33}(\Delta\hat{\beta}_3)^2 + 2(\Delta\hat{\beta}_1 d_{13} + \Delta\hat{\beta}_2 d_{23})\Delta\hat{\beta}_3 + d_{11}(\Delta\hat{\beta}_1)^2 +$$

$$2d_{12}\Delta\hat{\beta}_1\Delta\hat{\beta}_2 + d_{22}(\Delta\hat{\beta}_2)^2 - 3F\alpha\,(3,33) = 0 \qquad \text{(IV.12)}$$

In this relation d_{ij} is an element of the inverse of the matrix $\mathcal{X}$.

The projection of the ellipsoid on the β_1-β_2 plane is formed by the values of $\Delta\hat{\beta}_1$ and $\Delta\hat{\beta}_2$ for which relation IV.12 has only one solution to $\Delta\hat{\beta}_3$. The formula of this projection is:

$$(\Delta\hat{\beta}_1)^2((d_{13})^2 - d_{11}d_{33}) + 2\Delta\hat{\beta}_2(d_{13}d_{23} - d_{12}d_{33})\Delta\hat{\beta}_1 +$$

$$(\Delta\hat{\beta}_2)^2((d_{23})^2 - d_{22}d_{33}) + 3F\alpha(3,33) = 0 \qquad \text{(IV.13)}$$

For fixed $\Delta\hat{\beta}_2$ values, $\Delta\hat{\beta}_1$ can be solved directly from equation IV.13.

LITERATURE APPENDIX IV

1) Linssen,H.N., Internal Report Eindhoven University of Technology, Department of Mathematics, 1973.
2) Behnken,D.W., J.Polymer Sci.A, 2,645 (1964).
3) Draper,N.R., and Smith,H., "Applied Regression Analysis". Wiley, New York, 1967.

LIST OF SYMBOLS

		units*
A	parameter of equation 5.5	$l(g\ cat\ sec)^{-1}$
B	parameter of equation 5.5	$l^2(g\ cat\ sec)^{-2}$
c, c_{EB}	concentration of ethylbenzene	$mmol\ l^{-1}$
c_{St}, c_H	concentration of styrene and hydrogen respectively	$mmol\ l^{-1}$
c_o, c_{Sto}, c_{Ho}	initial concentration of ethylbenzene, styrene and hydrogen respectively	$mmol\ l^{-1}$
D_a	axial dispersion coefficient	$cm^2\ sec^{-1}$
D	molecular diffusion coefficient of ethylbenzene in carbondioxide	$cm^2\ sec^{-1}$
F	gas flow rate	$l\ h^{-1}$, $l\ sec^{-1}$
k	reaction rate constant	$l(g\ cat\ sec)^{-1}$
k_{eq}	equilibrium constant	$mmol\ l^{-1}$
KE, KS, KH	adsorption equilibrium constant of ethylbenzene, styrene and hydrogen respectively	$l\ mmol^{-1}$
L	length of the catalyst bed	cm
n	reaction order, number of recirculations	
r	rate of reaction	$mmol(g\ cat\ sec)^{-1}$

t	time	sec, min
T	temperature	^{o}C, K
u	linear gas velocity	cm sec^{-1}
W	catalyst weight	g
x_{EB}, x_{H2}	mole fraction of ethylbenzene and hydrogen	
α	degree of reduction of the catalyst, statistical probability level	
β_o	parameter of equation 5.14	g cat sec $mmol^{-1}$
β_1	parameter of equation 5.14	g cat sec l^{-1}

*unless stated otherwise

SUMMARY

For the dehydrogenation of ethylbenzene to styrene a new and effective catalyst - uraniumdioxide UO_2 - has been found. The reaction has been investigated over pure UO_2 and over UO_2 on alumina in an inert atmosphere in the temperature range of 450 - 520°C. The active catalyst is prepared by reduction of U_3O_8 containing catalyst with ethylbenzene under reaction conditions. During the reduction, carbondioxide, water, benzene, toluene and styrene are formed. After complete reduction, the catalyst consists of $UO_{2.00}$ (with or without support), and yields styrene and hydrogen from ethylbenzene with selectivities of over 95% at high degrees of conversion. The reductions of both pure uranium oxide and uranium oxide on alumina with ethylbenzene and with hydrogen have been studied in a thermobalance.

The kinetics of the dehydrogenation reaction over UO_2 on alumina were studied in a special type of reactor, which is operated as a continuous stirred gas solid reactor (CSGSR) and as a fixed bed reactor, and which can be switched over easily from the one mode of operation to the other.

Differential and integral fixed bed experiments showed that the dehydrogenation rate can be described by:

$$r = \frac{k(c_{EB} - c_H c_{St}/k_{eq})}{1+KEc_{EB}+KSc_{St}}$$

After the observed data were corrected for non-ideal flow in the plug flow reactor and in the CSGSR the experimental results of both reactor types were described excellently with one set of estimates for the parameters k, KE and KS. A statistical analysis of the kinetic results is made; the confidence regions of the parameter estimates are given.

From estimates of rate constant k an activation energy of 23 kcal mol^{-1} is calculated. Because of the high relative errors of the estimates of KE and KS no heats of ad-

sorption for ethylbenzene and styrene are calculated.

The hydrogenation-dehydrogenation reaction takes place on one complex UO_2 site on which ethylbenzene or styrene and hydrogen are adsorbed. Analogously to hydrogenation-dehydrogenation reactions on chromia and zincoxide the following mechanism for the dehydrogenation of ethylbenzene on uraniumdioxide is proposed:

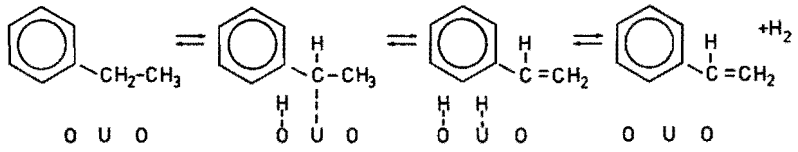

SAMENVATTING

Voor de dehydrogenering van ethylbenzeen tot styreen is een nieuwe katalysator - uraniumdioxide UO_2 - gevonden. De reactie is onderzocht over zuiver UO_2 en over UO_2 op aluminiumoxide in een inerte atmosfeer bij temperaturen van 450 - 520°C. De dehydrogeneringskatalysator wordt bereid door reductie van U_3O_8 bevattende katalysator met ethylbenzeen onder reactiecondities. Tijdens deze reductie worden kooldioxide, water, benzeen, tolueen en styreen gevormd. Na reductie bestaat de katalysator uit $UO_{2,00}$ (met of zonder drager) en geeft styreen en waterstof uit ethylbenzeen met selectiviteiten boven 95%, zelfs bij hoge conversiegraden. De reducties van zuiver uraniumoxide en van uraniumoxide op aluminiumoxide met ethylbenzeen en met waterstof zijn onderzocht in een thermobalans.

De kinetiek van de dehydrogeneringsreactie over UO_2 op aluminiumoxide is bestudeerd in een speciale reactor, die als continu geroerde gas-vastestof-reactor (CSGSR) of als propstroomreactor kan worden bedreven, en die gemakkelijk kan worden overgeschakeld van het ene reactortype naar het andere.

Uit differentiële en integrale propstroomexperimenten is gebleken dat de dehydrogeneringssnelheid kan worden beschreven met:

$$r = \frac{k(c_{EB} - c_H c_{St}/k_{eq})}{1 + KEc_{EB} + KSc_{St}}$$

Nadat de metingen gecorrigeerd zijn voor niet ideale stroming in de CSGSR en de propstroomreactor, is het mogelijk de experimentele resultaten van beide reactoren te beschrijven met één stel schatters van de parameters k, KE en KS. Een statistische analyse van de resultaten van de kinetische metingen is gemaakt, en betrouwbaarheidsgebieden voor de parameterschatters zijn gegeven. Met behulp van de schat-

ters van de reactiesnelheidsconstanten k wordt een activeringsenergie van 23 kcal mol^{-1} berekend. Omdat de fouten in de schatters van KE en KS relatief groot zijn, zijn geen adsorptiewarmten voor ethylbenzeen en styreen berekend.

De hydrogenerings- of dehydrogeneringsreactie treedt op aan één complexe UO_2 site waarop ethylbenzeen of styreen en waterstof geadsorbeerd worden. Analoog aan hydrogenerings-dehydrogeneringsreacties over chroom- en zinkoxide wordt voor de ethylbenzeendehydrogenering over uraniumdioxide het volgende mechanisme voorgesteld:

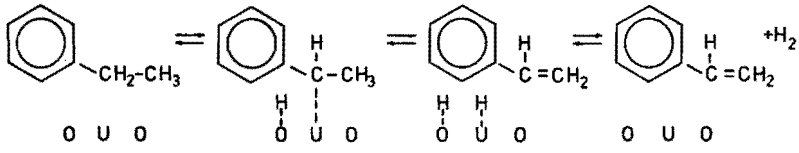

DANKWOORD

Dit proefschrift is tot stand gekomen door de samenwerking van alle leden van de vakgroep chemische technologie. In het bijzonder wil ik hier noemen mevrouw C.G.M.M. Camp-van Berkel, die met grote toewijding heeft meegewerkt aan het onderzoek, evenals de afstudeerders H.G.A.Coenen, W.N.Ch.Heeren, J.A. van Heugten, J.G.Lamkin, A.M.H.Jonker en M.J.H. van de Weyer. R.J.M. van der Wey en D.Francois ben ik erkentelijk voor het ontwerp en de opbouw alsmede het onderhoud van reactoren en apparatuur. R.Kool is een grote steun geweest bij de computerberekeningen en H.N. Linssen heeft waardevolle adviezen gegeven bij de statistische verwerking van de meetresultaten. De Engelse tekst werd gecorrigeerd door H.J.A. van Beckum, de tekeningen werden gemaakt door P.F.Hermans en mevrouw P.M.Th.Tilmans-Berger heeft een groot gedeelte van het manuscript getypt. Aan allen, ook diegenen die ik hier niet bij naam heb genoemd, mijn hartelijke dank.

LEVENSBERICHT

De schrijver van dit proefschrift werd op 11 februari 1946 te Heinsberg (Dld.) geboren. Hij bezocht de MULO-school te Sittard en behaalde in 1961 de diploma's MULO-A en B. Vervolgens verwierf hij in 1965 te Heerlen het HTS-diploma Chemische Techniek. September 1965 werd hij als student ingeschreven aan de Technische Hogeschool Eindhoven, afdeling der Scheikundige Technologie, waar hij na een afstudeerperiode bij Prof.drs.H.S. van der Baan in juni 1969 het ingenieursdiploma behaalde. Sindsdien is hij als wetenschappelijk medewerker werkzaam in de groep chemische technologie van de Technische Hogeschool Eindhoven. Na afronding van het afstudeeronderzoek naar de continue katalytische dimerisatie van oliezuur werd in 1971 met het onderzoek, in dit proefschrift beschreven, gestart.

STELLINGEN

1. Cadmiumoxide is niet geschikt als katalysator voor de oxidatieve dealkylering van methylnaftalenen in continu doorstroomde reactoren.

   C.J.Norton en T.E.Moss, U.S.Patent 3175016 (1965).

2. De suggestie van Bell dat de aciditeit van een geconcentreerde oplossing van een sterk zuur evenredig is met de zuurconcentratie en omgekeerd evenredig is met de vierde macht van de waterconcentratie is onwaarschijnlijk.

   R.P.Bell, "Acids and Bases", Methuen and Co. Ltd., London, 1969, p.47-51.
   R.P.Bell, "The Proton in Chemistry", Methuen and Co. Ltd., London, 1959, p.74-86.

3. In het infraroodspectrum van hogedrukpolytheen wordt de absorptieband bij 893 cm^{-1} ten onrechte aan methylgroepen toegeschreven.

   D.O.Hummel, "Atlas der Kunststoff-Analyse", Carl Hanser Verlag, München, 1968, p.125.

4. Om de waarde van kinetische experimenten beter te kunnen beoordelen zou er meer gebruik moeten worden gemaakt van intervalschatters in plaats van puntschatters.

5. Het mathematische model voor sproeidrogen van Parti en Paláncz zal in de praktijk tot onderschatting van de droogtijd en daardoor tot onderdimensionering van de sproeidroogapparatuur leiden.

   M.Parti en B.Paláncz, Chem. Eng. Sci. 29, 355 (1974).

6. Het is hoogst onwaarschijnlijk dat de laatste piek in het chromatogram van het door Céntola et al. beschreven propeen epoxidatie productmengsel, bestaande uit onder andere aceetaldehyde , propyleenoxide, propionaldehyde, acroleine en formaldehyde, kan worden toegeschreven aan formaldehyde.

   P.Céntola, C.Mazzocchia, G.Terzaghi en I.Pasquon, Chim.Ind. (Milan) 54, 859, (1972).

7. Het huidige omvangrijke arsenaal van analyse- en rekentuig brengt met zich mee dat het gevecht om Moeder Natuur haar geheimen te ontfutselen meer het karakter krijgt van een slijtageslag dan van een weloverwogen tactische operatie.

8. Het is te betreuren dat nu ook officiële regeringspublicaties de sombere - maar mogelijk reeds achterhaalde - mededelingen van de Koninklijke Nederlandse Chemische Vereniging over plaatsingsmogelijkheden voor scheikundige ingenieurs, als waarheid verkondigen.

   Straks studeren? Publicatie van het Ministerie van Onderwijs en Wetenschappen, zevende jaargang, nummer 1, 1974.

9. Het verdient aanbeveling om voor een wandeling over de Strabrechtse heide een zodanige route te kiezen dat men het hoofd minstens een kwart slag moet draaien om zich te kunnen oriënteren op de, de horizon beheersende, Geldropse flatgebouwen.

10. Een promovendus kan niet zonder een laatste stelling.

Eindhoven, 24 september 1974. G.Heynen